DYNAMICS MODELING AND CONTROL SYSTEM DESIGN FOR SHAPE MEMORY ALLOY ACTUATORS

IN SEON KIM

A THESIS SUBMITTED TO THE FACULTY OF GRADUATE STUDIES
IN PARTIAL FULFILMENT OF THE REQUIREMENTS
FOR THE DEGREE OF

MASTER OF SCIENCE

GRADUATE PROGRAM IN EARTH AND SPACE SCIENCE
YORK UNIVERSITY
TORONTO, ONTARIO
DECEMBER 2014

Abstract

Shape memory alloy (SMA) is a type of smart material which remembers its original state. It is light weight and small, and known to provide high contraction force with low noise. Its application has wide range from robotics to medical science. One of its potential applications in space is a supporting system of membrane structure that can be used as synthetic aperture radar (SAR) antenna to achieve high flatness. It exhibits nonlinear phenomena called hysteresis when it's electrically heated. Hysteresis is a nonlinear phenomenon that refers to the dependence of a physical system on the environment. Hysteresis in SMA causes a major difficulty in control system design. Un-modeled or poorly modeled hysteresis introduces inaccuracy in tracking and the performance of the system.

A experimental test bench is constructed for one set of SMA actuators that resembles the membrane structure's supporting system. Hysteresis is obtained by running open loop test with the test bench. Dynamics model of the SMA wires is developed using classical Preisach model and modified Maxwell model. Then

the inverse model is implemented in feed-forward loop to compensate for nonlinear hysteresis. Simple feedback controllers are added to correct the modeling errors.

Experimental results reveal that the error is significantly reduced when comparing feedback controller with hybrid feedback and feed-forward controller.

I dedicate this thesis to people I love who love me in return

Acknowledgements

I would like to acknowledge, with gratitude, Professor Jinjun Shan for his supervision. His advice and guidance was invaluable on completing this work.

Sincere thanks to my lab mates, Ryan Orszulik, Lei Liu, Yanfang Liu, Liu Yang, and Shawn Walker, for various help they have offered me.

Last, but certainly not least, I would like to thank my family and friends, my parents, Jong Deok Kim and Hyun Ju Yoo, my sister and brother, Hye Won Kim and Gi Yeon Kim, and my best friend, Luke O'Neill for their financial and mental support.

Table of Contents

List of Tables

List of Figures

1 Introduction

Shape memory alloy (SMA) is a smart material that remembers its original state. Its application has wide range from robotics to medical science. One of its potential applications in space is a supporting system of membrane structure that can be used as synthetic aperture radar (SAR) antenna to achieve high flatness. A test bench for SMA actuators that resembles the membrane system is constructed. Nonlinearity in SMA actuators can cause inaccuracy when tracking. Control system design containing dynamics modeling of hysteretic behavior of SMA actuators is developed. Dynamics model is developed by using classical Preisach model and modified Maxwell Resistive Capacitor (MRC) to compensate nonlinearity in SMA actuators. While classical Preisach model is a basic hysteresis model it requires long computation time. Maxwell model is a subsystem that is developed from the classical Preisach model. In the experiment, it is determined that modified Maxwell model is faster and more effective. Simulations for both dynamics model and its inverse model are conducted for verification. Inverse dynamics model is

implemented in feedforward controller to predict input value ahead for desired output value. Since dynamics model closely maps hysteresis of SMA actuators, a simple feedback controller can be utilized to compensate modeling error. Simple PI and $PI-P^3$ controllers are implemented. Experimental verification is performed to compare feedback-feedforward controller to feedback controller itself.

1.1 Characteristics, History, and Development of SMA

A Shape memory alloy is a type of smart material which remembers its original state. One of the commonly used SMA materials is Nickel-titanium, known as Nitinol. Nitinol stands for Nickel Titanium Naval Ordnance Laboratory. As the name suggests, it was discovered by a researcher, William J. Buehler, at the Naval Ordnance Laboratory in 1962. Soon after its discovery, it found applications in U.S. and British Navy to join titanium tubing using hydraulic couplings and moved its way up to scientific and robotics applications. When it is compared to other materials, Nitinol prevails to have greater ductility, more recoverable motion, good corrosion resistance, stable transformation temperatures, higher bio-compatibility, and ability to be electrically heated [10]. On the other hand, there lies a great challenge in control due to a phenomenon known as shape memory effect (SME). SME refers an ability to contract back to its original state when heated. In SMA, SME is nonlinear and dependent on the temperature and stress. It occurs as a result of

crystalline structure change due to temperature. Assume a SMA's original state is state "A" in Fig. 1.1. It has low temperature without applied force. Crystalline structure has parallelogram shape at this point. When heat is applied, its state transitions to "B". At "B", the length of the SMA shortens due to temperature increase, and crystalline structure deforms to cubical form. It does not come back to parallelogram shape like the original state even when heat is removed (state "C"). It finally comes back to its original form when heat is removed and force is applied. Nonlinear SME causes hysteresis in the system. Hysteresis refers to the dependence

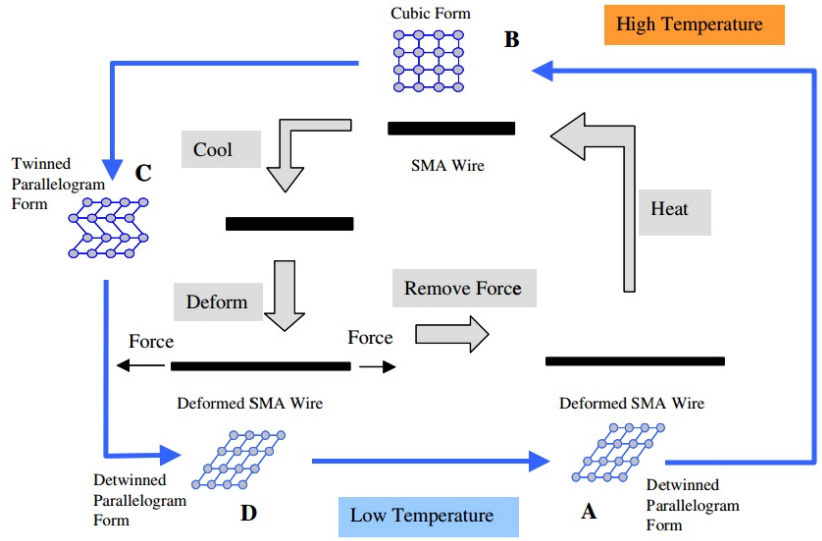

Fig. 1.1 Micro and macro view of SMA phase transformation [1]

of a physical system on the environment. The term "hysteresis" is introduced by James Alfred Ewing, a Scottish physicist in 19th century, as the persistent effects the temporary exposure of ferric metals to magnetic fields [13]. The term can be

found in various disciplines such as magnetics, electronics, and economics. When a SMA actuator deforms and comes back to its normal state, it does not always follow the same deformation process. Hysteresis loop is displayed when nonlinear deformation process is plotted, as shown in Fig. 1.2. It introduces unwanted inaccuracies when building a control system. Different behaviors of SMA in heating and cooling processes cannot be tracked with typical linear controller. Thus, it requires special techniques to achieve precision in control. Hysteresis loop can be divided into two transformation phases, austenite (A) and martensite (M) phases. Austenite phase begins from austenite start temperature, A_s, and finishes at austenite finish temperature, A_f, forming heating curve of the system. Martensite phase forms cooling curve of the system from martensite start temperature, M_s, to martensite finish temperature, M_f. This distinctive transformation causes hysteresis and introduces nonlinearity in the system. Since SME is dependent on temperature, the environ-

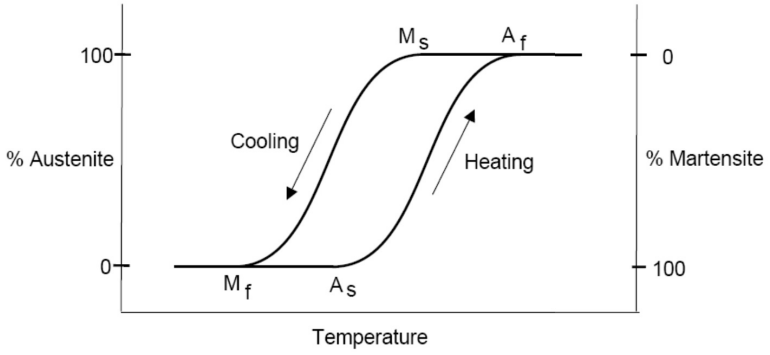

Fig. 1.2 SMA Transformation [2]

ment that the SMA system is in plays a crucial role. When the system is not in vacuum, it introduces heat transfer through air convection, disturbing its performance. Peng et al. [14] performed a test with a preliminary SMA test bench with dead weight bias and linear variable differential transformer (LDVT) displacement transducer. They compared actuators performance in vacuum and air. It was concluded that the current required for control in vacuum is less than that in air. They were able to achieve 95% energy saving. Furthermore, time delay in the process of heat diffusion and phase transformation was shorter when the power was removed. As a result, error was reduced by 43% in vacuum.

SMA is often used as an actuator. There are various way to arrange SMA actuators for different applications. By placing them in different manners, they allow the system to have flexible forms of operation. Fig. 1.3 shows the different SMA connection types: linear, spring, rotary, and bundle SMA actuators. Linear SMA actuator is the most basic configuration. It is simple and easy to be integrated with devices and structures. It also has faster response time than other configurations [3]. Linear connection of SMA wries found their applications in membrane wrinkle control [15], flexible beam control [16], and so on.

When SMA actuators are wired in spring form, it obtains properties of a spring as well as its original properties. Lee et al. [17] provide four test analyses of a spring actuator used for an active catheter. A SMA spring actuator is wound on a

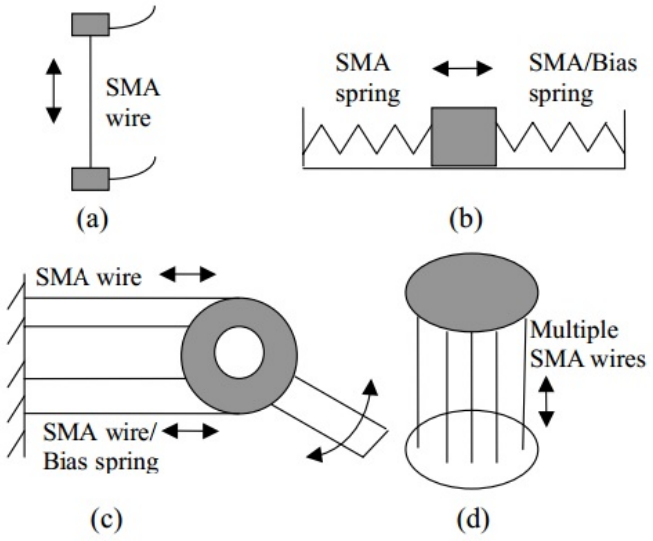

Fig. 1.3 (a) Linear SMA actuator (b) Spring SMA actuator (c) Rotary SMA actuator (d) Bundle SMA actuator [3]

mandrel and fabricated by the heat treatment. Their system was developed to be used in medical robots with high accuracy. Also Ishii and Ting [18] presented SMA actuated compliant bistable mechanisms with spring actuator that can preserve advantages of SMA and eliminates disadvantageous characteristics.

Rotary actuator is normally formed with pulley system or SMA strip in coil form [3]. It is tolerant to residual strains and suitable for meso or micro level robotic system. Generally, micro fabrication treatment is applied to enhance the bending of SMA actuator [3].

Performance of bundle actuators is dependent on wire diameter, number of wires, bundle length, and number of parallel current path. It can hold more load

than linear actuator, however, it requires more delicate control and voltage/current to operate.

Despite their attractive properties, challenges remain in control to maximize SMA's potentials. The challenges associated with controlling SMAs include hysteresis modeling and compensations, heat transfer, slow cooling process and so on.

1.2 Applications and Motivation

Due to the features such as high contraction force and low noise, SMA actuators found wide applications in various fields, from medical to robotics [19,20]. In space industry, cost per weight and volume to launch into space is very high. Hence, light weight and small actuators that can deliver high forces are always attractive features for space missions. Peng [15] gives possible applications of SMA actuators including the deployment system of membrane structure and rotating the glass cover of the solar panel of Mars Pathfinder "Sojourner" to avoid dust deposit on the panel during sandstorm on Mars. He also raises his concerns about difficulty using SMA actuators. A SMA actuator has poor stability and controllability. It is hard to achieve steady output even with the same input. It also has slow response speed and is hard to map hysteresis accurately. Response time can be improved by using thin SMA actuators. However, thin SMA actuators are more sensitive to environment. Careful tests and analyses must be made to accurately understand

its properties.

The Spacecraft Dynamics Control and Navigation Laboratory (SDCNLab) at York University possesses a world-class membrane structure test facility for investigation of active shape/flatness control of space membrane structures, which have potential applications in synthetic aperture radar (SAR) antenna, membrane mirrors, and so on. Fig. 1.4 shows the membrane test facility at SDCNLab.

Membrane is fabric like material. It needs to stay flat in order to be accurate and effective. However, when it is deployed in space, membrane is subject to wrinkling due to thermal and mechanical disturbances [15]. Having wrinkles affect performance negatively by introducing surface inaccuracy in membrane reflectors and/or nonuniform surface heating in solar sails. The general guideline suggests that the membrane maintains 1/10 to 1/20 of operation wavelength. Sets of SMA actuators are supporting membrane along the boundaries. It is optimal not to have sensors or actuators on the structure because they can interfere with microwave components and reduce the performance [4]. Uniformly placed 20 sets of SMA actuators hold membrane, provide boundary tensions to relieve wrinkles. High accuracy control of individual SMA is needed to achieve high flatness. The objectives of the research are to model the dynamics of SMA with nonlinearity accurately and design effective controller for tension control.

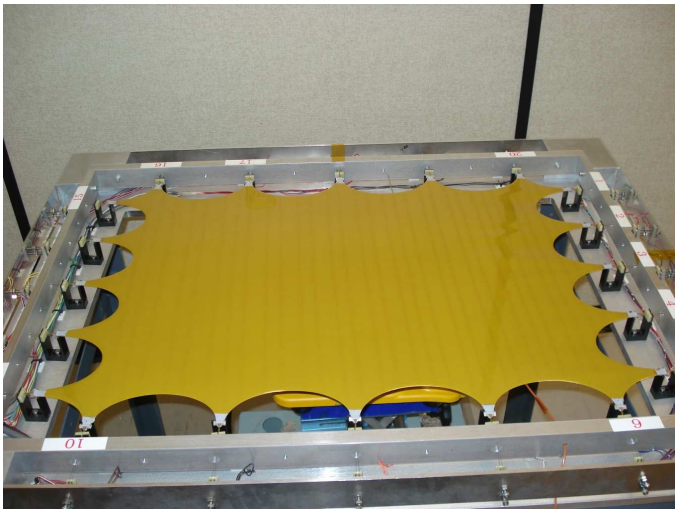

(a) Membrane structure

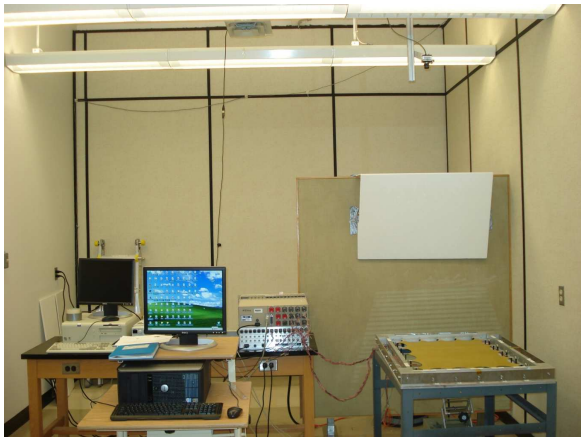

(b) Overall membrane system

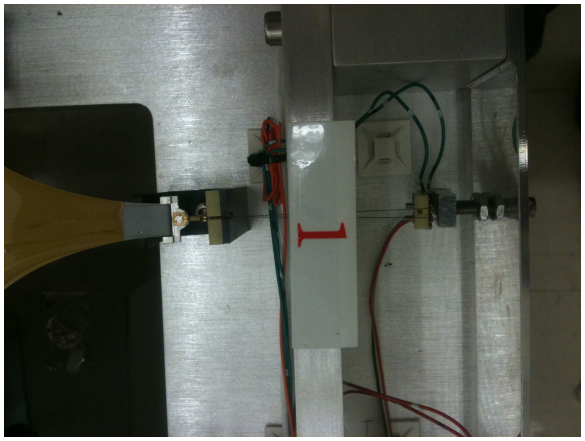

(c) 20 SMA actuators are used to support membrane structure

Fig. 1.4 Membrane experimental system at SDCNLab [4]

1.3 Experimental Setup

Despite the simplicity and effectiveness of the linear SMA actuator, refer to Fig. 1.3 (a), its nonlinearity prevents a precision control. A test bench with one set of SMA actuators is built for experiments. It was designed in a way that it resembles SMA structure in the membrane system in SDCNLab. The test bench consists of a set of SMA actuators (one set of SMA actuators is composed with two SMA actuators connected in parallel form), two support beams for SMA actuators (one for each end), a strain gauge, circuit board, National Instruments SCB-68 DAQ box, Ectron Corporation 563H board, and a computer for real time control. Fig. 1.5 shows the test bench. A flexible beam is connected by SMA actuators with a fixed beam. The fixed beam is secured on the platform with adjustable screw such that a desired pre-tension force can be adjusted. On the inner side of the flexible beam, a strain gauge is mounted and connected to Ectron board so when shortening of actuators' length triggers the beam bends and strain gauge reads tension force. The computer utilizes MATLAB and xPC target for real-time control. It reads strain gauge output from Ectron board and sends commands through NI card to apply current to SMA actuators. Current supply is connected to one end of SMA actuator and to circuit board which is connected to NI card and the other SMA actuator.

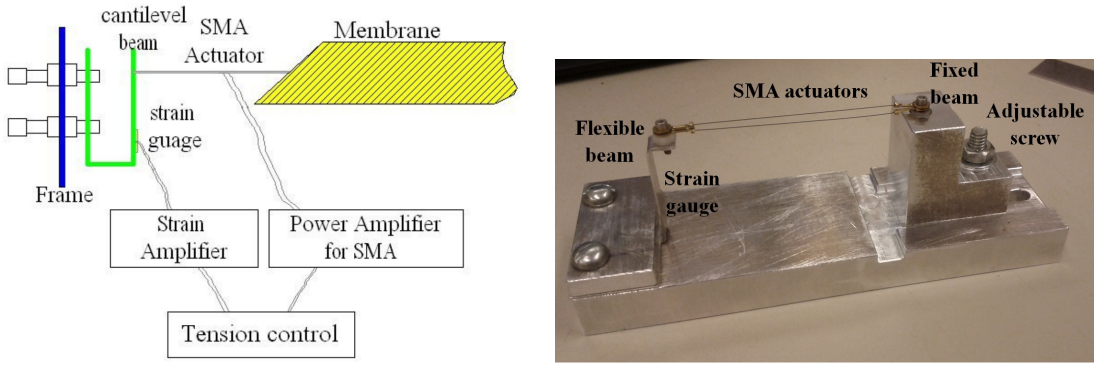

(a) Membrane SMA actuator connection [21] (b) Test bench built at SDCNLab

Fig. 1.5 SMA actuator connections

In this research, the material of the actuator is Nitinol (NiTi) which is the same as the SMA material used in the membrane system. This is because the objective of the research is to provide SMA control for the existing membrane structure. Properties of the SMA actuator is listed in Table 1.1.

Table 1.1 Properties of SMA actuators

Property	Value
Material	Nitinol (NiTi)
Diameter	0.2 mm
Length	66 mm
Resistance	29 Ω/m
Maximum Input Current	660 mA

The existing system relies on digital PWM signal as system input. However, it does not provide one-to-one relationship between input and output since it is simple on and off signal. In order to establish an accurate dynamics model, it is desired to provide analog signal as system input of the SMA test bench. A simple voltage

to current converter is built to generate the desired current from the input voltage in order to implement analog system. In Fig. 1.6, R_L represents the resistance of the SMA actuators. The applied current to SMA actuators are determined by the value of R_1 as

$$I_L = \frac{V_{in}}{R_1} \tag{1.1}$$

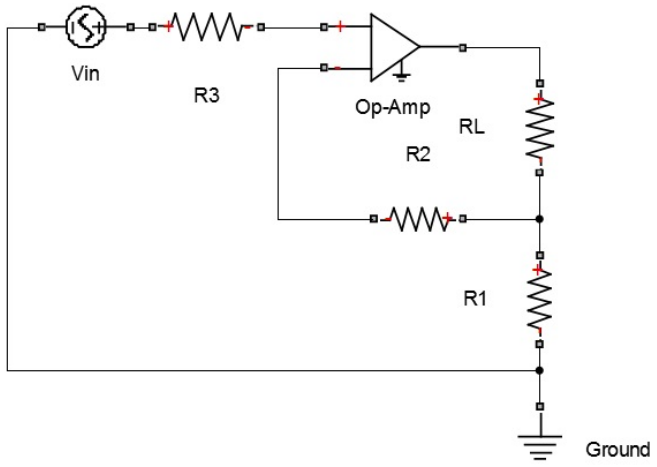

Fig. 1.6 Voltage to current converter

The overall system diagram is illustrated in Fig. 1.7, where V stands for voltage and I represents current.

It should be noted that the experimental system does not contain active cooling system. SMA actuators have slow cooling time, therefore, cooling of a SMA actuator is generally done by heat removal techniques in forms of heat sink, wa-

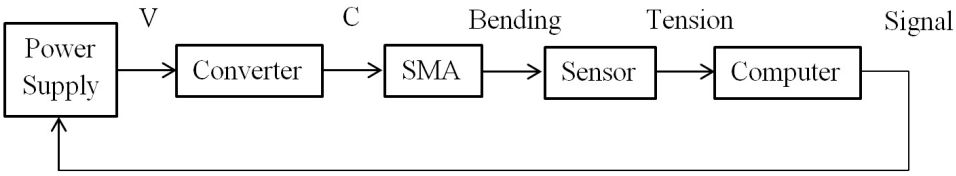

Fig. 1.7 Overall system process diagram

ter immersion, and forced convection. However, the membrane structure does not require fast cooling. Cooling of the experimental system will be done naturally by removing electrical current. Heating of the actuators are more important than cooling because heating causes greater tension in wire to stretch the membrane.

1.4 Contributions of this thesis

This thesis emphasizes on providing effective position control for SMA actuators. It is achieved with two main parts: dynamics modeling and control system design. The hysteresis in SMA is compensated for, by the dynamics model in feedforward control and feedback controller corrects the error. In this work, two dynamics models and two control methods will be studied.

In Chapter 2, the detailed models of physical process in a SMA actuator are introduced. It offers theoretical and mathematical procedures behind the suggested models. Heat transfer dynamics and hysteresis models are introduced. A transfer function is derived from time constant to compensate for the positive phase shift.

In Section 2.2, the hysteresis loop is identified and Preisach and Maxwell models are developed accordingly. The hysteresis of SMA is studied extensively by many researchers. However, many of them utilizes controllable power supply so stable one to one relation could be achieved between the output and the power input. The original system utilizes pulse width modulation (PWM) as the system input therefore it is hard to obtain stable and consistent hysteresis loop. For this research, voltage to current converter is implemented to replace the digital system input by an analog. The classical Preisach model and modified Maxwell model are studied and compared for modeling the hysteresis. The classical Preisach model is one of the most popular hysteresis models used for SMA. The Maxwell model is another conventional hysteresis model that is considered as sub-model of the classical Preisach model. The modifications are made to Maxwell model to accommodate irregularity in hysteresis loop. Furthermore, in Section 2.3, techniques used to identify parameters from the experimental data for the classical Preisach model and the modified Maxwell model are explored. The parameter identification method, as well as the identified results are given. Simulation data from both hysteresis models are provided, analyzed, and compared.

In Section 3.2.2, the inverse model of the modified Maxwell model is developed. The inverse model can be used in a feedforward control loop and compensate for the nonlinear hysteresis effect in a SMA actuator. Verification results are presented.

In Chapter 3, the development of control system of SMA actuators is discussed. Background information is provided from literature review. Section 3.1 introduces control methods suggested by researchers. It includes linear and nonlinear systems with different control techniques. In Section 3.2, feedforward controller coupled with a simple feedback controller is suggested for this research. Feedforward term compensates the hysteresis effect in SMA actuators and feedback controller corrects the modeling error. The controller is tested with the test bench and the results are compared.

Chapter 4 concludes this thesis and states future work to be done.

2 Dynamics Modeling of SMA

2.1 Background

There are various physical properties and dynamic processes involved in a SMA actuator system. Depending on its application and how the system is setup, heat transfer, phase transformation between temperature and stress, strain, and electrical resistance exist in the system. This chapter focuses on modeling of two dynamic processes, heat transfer and phase transformation of a shape memory alloy. The heat transfer occurs between input current and temperature, while the phase transformation involves hysterectic behavior of SMA actuators.

2.1.1 Heat Transfer

SMA actuators are activated mostly by heat transfer. Heat energy is obtained by electric current and easily affected by environment through natural convection. Heat transfer characteristics are important and needs to be analyzed to achieve accurate tracking. The relationship between temperature and potential difference

of SMA wire is governed by the following lumped parameter convective heat transfer equation [22].

$$\rho c \frac{\pi d_0^2 L_0}{4} \frac{dT}{dt} = vi - \pi d_0 L_0 h (T - T_0) \tag{2.1}$$

where d_0 is the cross-sectional diameter of the undeformed wire (m), L_0 is undeformed SMA wire length (m), T_0 is the ambient temperature (K), ρ is the mass density of the wire (kg/m), c is the specific heat of the wire (J/K), vi is electric power (W), and h is the convective heat transfer coefficient of the wire (W/m^{2}K). Specific heat is a function of temperature, however, it is treated as constant value for simplification purpose. This simplification does not introduce error in the system because environmental disturbance is greater than the error caused by the simplification. This equation is useful when temperature is not measured directly from the SMA actuators. It offers mathematical estimation of temperature based on the input value.

Compared to heating, cooling is more sensitive to environment. Cooling can be achieved by natural air convection to remove heat from the system. Even though heat removal is the simplest method, there is no control over the cooling process since it is done naturally. If an application requires fast cooling, various cooling techniques can be applied. The commonly used cooling mechanisms include heat sink, water immersion, and forced convection. Researchers understood that response can be improved by having controlled cooling environment. Experiments

with mobile heat sink as cooling system of SMA actuators performed by Russel and Gorbet [23] show great improvement in speed and range of dynamic motion over the system without mobile heat sink. Lewis et al. [24] analyzed the behaviors of SMA actuator to study its functionalities under controlled convection. They acknowledged that the system's response time is affected by the influenced heating and cooling time. Factors that affect heating and cooling time include temperature, environment, convection of the environment, and the surface to volume ratio of the SMA wires. It ultimately creates nonlinearity in the system.

2.1.2 Hysteresis Models

Hysteresis is one of the most important characteristics of SMA for control purpose. A dynamics model of the SMA actuator is crucial for tracking. Various hysteresis modeling techniques have been investigated by many researchers [5, 6, 8, 25, 26]. There are two main approaches for hysteresis modeling. One approach relies on adapting the mathematical model to experimental data rather than deriving mathematical relationship from physical properties. Deriving mathematical model for the system requires complete understanding of the system and it can be very complex. The first method is often preferred for simplicity and high accuracy. Hysteresis models investigated in this section employs the approach that adapts the model to the experimental data. They have properties such as rate-

independence and memory effect. The term, rate-independence, implies that the input-output relationship is invariant with respect to the frequency or change rate of the input signal. Memory effect means that the output at a given time instant depends not only on the input value at that moment, but also on the historical input.

Classical Preisach Model

Ferenc Preisach first introduced Preisach model in 1935 to describe the hysteresis in ferromagnetic materials. It was further developed mathemetically by Krasnosepskii and other Russian mathematician groups [27]. Now it is one of the most popular hysteresis models due to its proven ability to accurately model a class of hysteresis. It describes physical phenomena with nonlinear hysteresis behavior [28] and reveals properties of hysteresis loop. It is an operator based hysteresis model that also serves as the basis for some other hysteresis models.

Preisach model describes hysteresis as a linear combination of weight function and relays. Each relay hysteron consists of an operator that switches between two values: α and β. α and β correspond to "up" and "down" switching values as illustrated in Fig. 2.1. The purely mathematical description of the Preisach model can be considered as an operator that integrates infinite weighted elementary

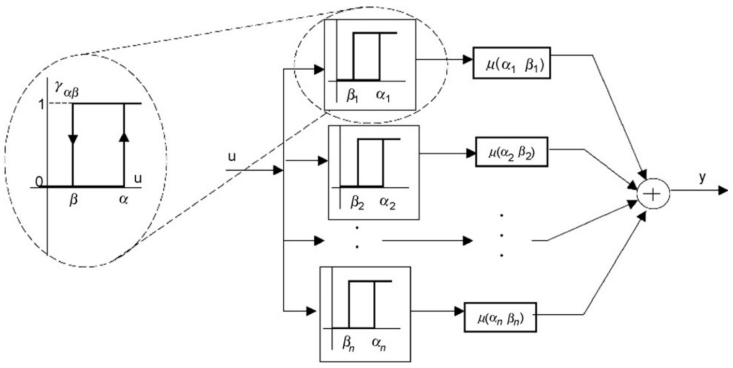

Fig. 2.1 Relay hysterons [5]

hysteresis operators $\gamma_{\alpha,\beta}$ over two dimensional region. It is expressed as

$$y(t) = \iint_{\alpha \geq \beta} \mu(\alpha, \beta)\gamma_{\alpha,\beta}[u(t)]d\alpha d\beta \tag{2.2}$$

where $\gamma_{\alpha,\beta}$ denotes the Preisach plane switching operator and $\mu(\alpha, \beta)$ is a weight function of α and β. Fig. 2.1 shows the finite dimensional approximation, which will be explained in more detail in Section 2.2.2.

Preisach plane offers geometric interpretation of relay hysterons. It covers triangular area when $\alpha \geq \beta$. α, β pairs from all relay hysteron are mapped and evaluated based on the input value. The coordinates outside of the Preisach plane are considered to be 0. Preisach model switches plane and adjusts output value between 0 and 1 as input value changes as follows,

$$\gamma_{\alpha,\beta} = \begin{cases} 0, & \text{if } u_t \leq \beta \\ 1, & \text{if } u_t \geq \alpha \\ r, & \text{if } \beta < u_t < \alpha \end{cases} \tag{2.3}$$

where u_t is the input value at current time t, r is 1 if u_{t-1} is greater than α, and is

0 if u_{t-1} is less than β. Fig. 2.2 illustrates active Preisach plane switching. In this

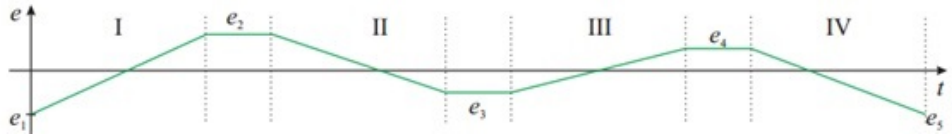

(a) Slope of an input example u(t)

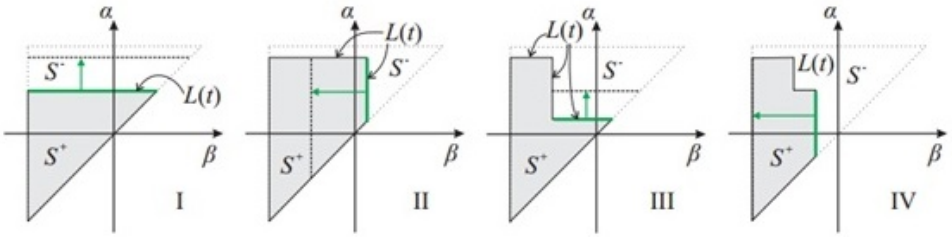

(b) Preisach plane with actibated (S+) and not activated (S-) switching operators

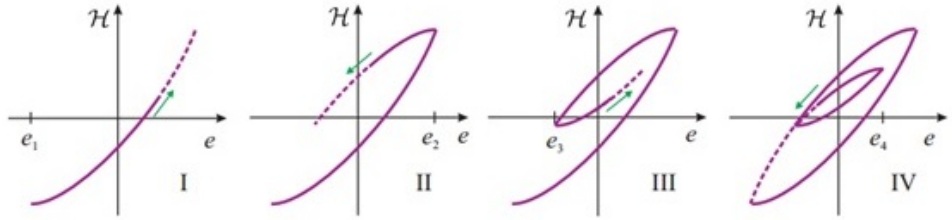

(c) Resulting hysteresis curve

Fig. 2.2 Preisach plane switching [6]

figure, e represents input value, S^+ is the area corresponding to switch-on status, S^- denotes switch-off status. Lastly, Fig. 2.2 (c) shows input-output hysteresis plot. When input value starts from e_1 and increases to e_2, S^+ area increases along α axis because more $\gamma_{\alpha,\beta}$ components are switched on. Phase II in this figure displays decreasing input value. As input value decreases, S^- area increases because $\gamma_{\alpha,\beta}$

components are switched off along β. This cycle repeats as input value changes. As a system runs, boundary line between S^+ and S^- becomes staircase line with horizontal lines correspond to local maxima of α and vertical lines correspond to local minima of β.

Weight function is a factor that determines the shape of hysteresis curve. Many weight functions have been utilized for different applications [5, 25, 29–31]. Some popular choices include the first order reversal curves (FORC), Gaussian density function, Lorentzian function, and derivative arc tangent (DAT) weight function.

FORC is introduced as a hysteresis data analysis tool [32]. It is in high demand for applications that require high accuracy because it is a proven method with great sensitivity and multitude of data that it can provide. However, it is not widely used due to its complexity. In data analysis and calculations, careful understanding of the procedures and results is required [31]. FORC originated in the classical Preisach model identification technique and therefore is often described as a slightly distorted Preisach distribution [31]. FORC is collected by changing the sample data field. FORC diagram starts from positively saturating field. Then, a sample is decreased to a reversal field, denoted by H_a. Lastly, it is increased again to H_b and returns to the positive saturation. FORC distribution is given as follows [32]:

$$\rho(H_a, H_b) = -\frac{\partial M(H_a, H_b)}{\partial H_a \partial H_b} \tag{2.4}$$

where $M(H_a, H_b)$ is measured magnetization. FORC diagram forms an experimen-

tal curves confined inside the major hysteresis loop (MHL) as shown in Fig. 2.3. Gaussian density function and Lorentzian function are analytical functions that

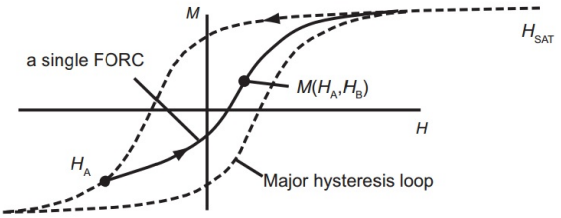

(a) Single FORC curve

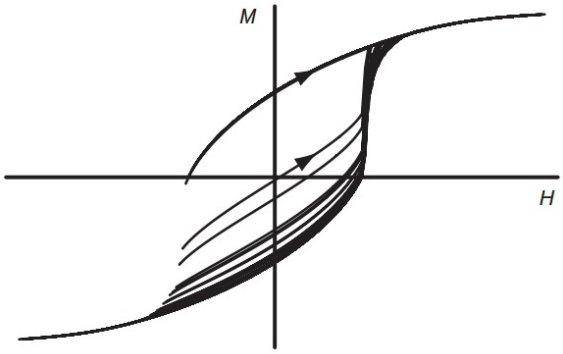

(b) Series of FORC curves

Fig. 2.3 FORC diagram [7]

express continuous weight function. They share the same parameters: A, h, σ_1, and σ_2, where A is normalization factor, and h, σ_1, and σ_2 are the characteristic parameters of the distribution [30]

$$\mu(\alpha,\beta)_{Gaussian} = A\exp\left(-\frac{1}{2}\left[\left(\frac{\beta-\alpha-2h}{2h}\sigma_1\right)^2+\left(\frac{\beta+\alpha}{2h}\sigma_2\right)^2\right]\right) \tag{2.5}$$

$$\mu(\alpha,\beta)_{Lorentzian} = A\frac{1}{1+\left(\frac{\alpha+h}{h}\sigma_1\right)^2}\frac{1}{1+\left(\frac{\beta-h}{h}\sigma_2\right)^2} \tag{2.6}$$

DAT weight function is developed based on the fact that the general shape of the outer hysteresis loop is arc tangent-like [30]. It is similar to Gaussian and Lorentzian, however, it has one additional term η

$$\mu_{DAT}(\alpha, \beta) = \frac{A}{1 + \{[(\alpha + \beta)\sigma_1]^2 + [(\alpha - \beta - h)\sigma_2]^2\}^{\eta}} \tag{2.7}$$

where η is introduced to allow the function to have more flexibility in shaping the corners of the hysteresis loop.

Prandtl-Ishlinskii Model

Prandtl-Ishlinskii (PI) model is also an operator based hysteresis model like Preisach model. It is desirable for its simplicity, ease of implementation and accuracy [33]. PI model employs a superposition of elementary "play" or "stop" operators that are continuous elementary operators [34]. Like Preisach model, it utilizes the sum of multiple operators.

Mathematical expressions of play operator F_r and stop operator E_r are defined in the literature [35]

$$\begin{array}{lll}
F_r[v](0) = f_r(v(0), 0) = w(0) & & \\
F_r[v](t) = f_r(v(t), F_r[v](t_i)); & t_i < t < t_{t+1} & \text{and } 0 \le i \le N-1 \\
E_r[v](0) = e_r(v(0)) & & \\
E_r[v](t) = e_r(v(t) - v(t_i) + E_r[v](t_i)); & \text{for } t_i < t < t_{t+1} & \text{and } 0 \le i \le N-1
\end{array} \tag{2.8}$$

where $f_r(v, w) = \max(v - r, \min(v + r, w))$, and $e_r(v) = \min(r, \max(-r, v))$. Play and stop operators are continuous and rate independent operators that decide the

slope of the hysteresis curve. They are a function of input v and the threshold r [34]. Play and stop operators are illustrated in Fig. 2.4

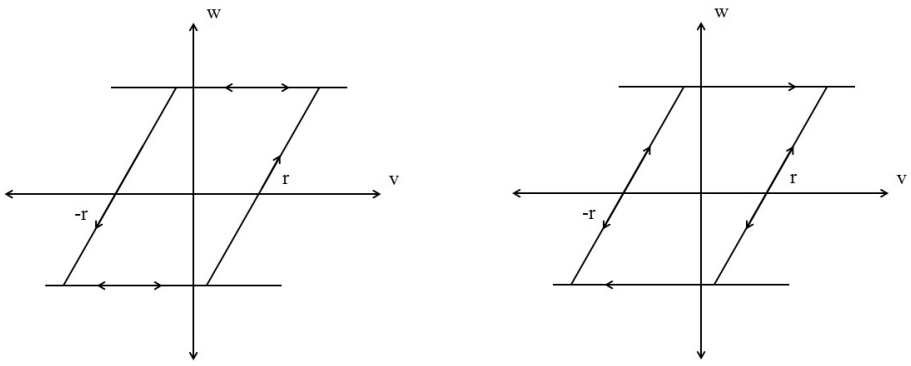

(a) Play operator (b) Stop operator

Fig. 2.4 Prandtl-Ishlinskii operators

Duhem Model

The Duhem model is a differential equation based hysteresis model that utilizes the fact that output has different characteristics for varying input. The Duhem model has been used to identify hysteresis in various smart materials and it has been proven that it can cover a large class of rate independency. It is capable of providing a finite-dimensional differential hysteresis model [36]. Differential equation of the Duhem model is

$$\frac{d\omega}{dt} = \alpha \left| \frac{dv}{dt} \right| [f(v) - \omega] + \frac{dv}{dt} g(v) \tag{2.9}$$

where α is a constant greater than 0, v is input, ω is output, and $f(v)$ and $g(v)$ are continuous functions. $f(v)$ is a piecewise smooth, monotone increasing, odd function with limited finite derivative $f'(v)$

$$f(v) = -f(-v), \lim_{v\to\infty} f'(v) < \infty \tag{2.10}$$

g(v) is a piecewise continuous even function with finite limit

$$g(v) = g(-v), \lim_{v\to\infty} g(v) = \lim_{v\to\infty} f'(v) \tag{2.11}$$

Like the Preisach model, the Duhem model is rate independent and has local memory. It also has inverse model that can be used for hysteresis compensation. By choosing appropriate $f(v)$ and $g(v)$ values, hysteresis can be established. This formulation can be easily modified to confine input-output relationship to a loop-like set.

Maxwell Model

Maxwell resistive capacitor (MRC) or Maxwell slip model is a variance of Preisach model [37]. Basic MRC operator originated from an elementary stop hysteron [38]. MRC, formulated by James C. Maxwell, consists of series of elasto-slide elements. Each elasto-slide elements have different stiffness and damping [39]. It is a friction model that distinguishes two regimes: slip and stick. In stick regime, absolute displacement is less than breakaway displacement. As an element in-

creases/decreases its displacement, it reaches breakaway displacement and enters slip regime. It is illustrated in Fig. 2.5.

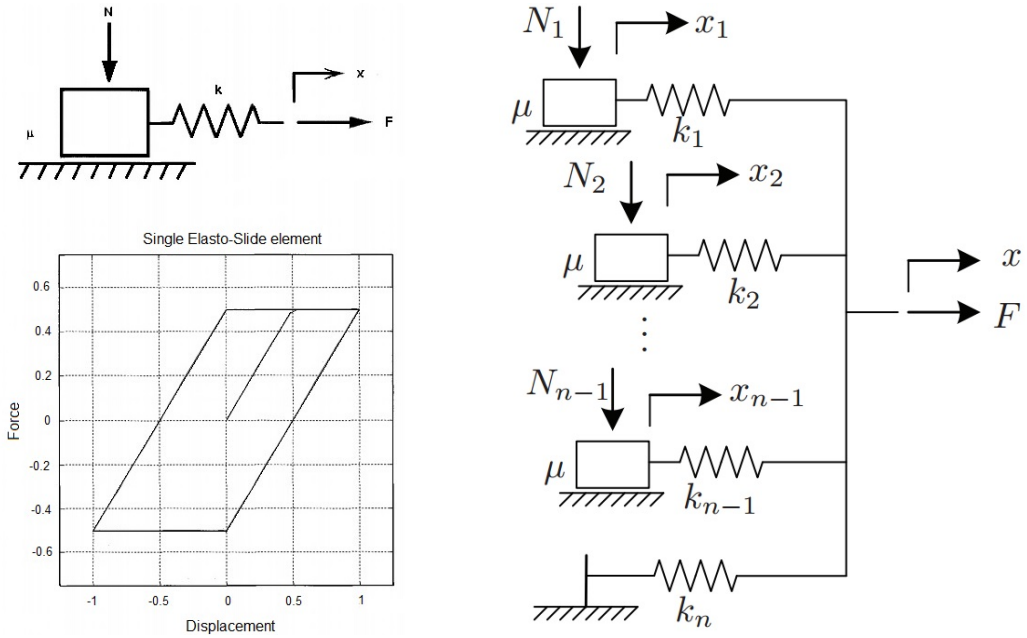

(a) Single Maxwell slip element (b) Maxwell slip elements in series

Fig. 2.5 Maxwell slip element [8]

Goldfarb and Calanovic [8] proposed a generalized MRC as a lumped-parameter causal representation of rate-independent hysteresis. In their paper, they describe single Maxwell slip element behavior as

$$F_i = \begin{cases} k_i(x - x_{b_i}), & \text{if } |k_i(x - x_{b_i})| < f_i \\ f_i \text{sgn}(\dot{x}) \text{ and } x_{b_i} = x - \frac{f_i}{k_i}\text{sgn}(\dot{x}), & \text{else} \end{cases} \tag{2.12}$$

where x is the input displacement, F_i is the output force, k_i is the spring stiffness, f_i is the breakaway force, and x_{b_i} is the block position for the i-th elasto-slide element.

When in series, the final output force, F, is

$$F = \sum_{i=1}^{n} F_i \tag{2.13}$$

The discrete version of Eq. (2.13) is [39]

$$\delta_i(t+1) = \begin{cases} sgn[x(t+1) - x(t) + \delta_i] \cdot |x(t+1) - x(t) + \delta_i(t)|, & \text{stick} \\ sgn[\delta_i(t)] \cdot \Delta_i, & \text{slip} \end{cases} \tag{2.14}$$

where δ_i denotes the current spring deformation and Δ_i denotes the maximum spring deformation. When a force is applied, the distribution is unknown. An iteration is used to calculate the distribution. It is assumed that each element has certain amount of force. Once one stiffness is identified, distributed force is proportional to each other (only when the system is not saturated).

2.2 Hysteresis Modeling

Hysteresis in SMA causes a major difficulty in control system design. Implementing precise hysteresis model in feedforward loop allows controller to compensate for the nonlinear hysteresis. Unmodeled or poorly modeled hysteresis introduces inaccuracy in tracking system performance [40]. In this section, Preisach and Maxwell models are developed for hysteresis compensation. These two models are selected for the following reasons. Preisach model is one common hysteresis model for SMA actuators. Its ability to closely identify complex hysteresis attracted many researchers. Maxwell model is also a popular hysteresis model, which consists of

multiple Maxwell slip elements so that it is easy to obtain accurate tracking. In SMA, hysteresis exists in phase transformation between temperature and stress. Hysteresis models are used to map the temperature-stress relationship.

2.2.1 Problem Statement

The existing SMA system on membrane structure relies on digital (PWM) signal as system input. While PWM signal is an effective and proven tool to reduce the energy consumption and deliver good performance for feedback controller, it does not provide one-to-one relationship between the input and output. PWM is essentially on and off signal. Thus specific input voltage cannot be estimated which makes it hard to generate consistent output. As it is illustrated in Fig. 2.6, the generated output signal is noisy and the response time to applied input current is very slow. It creates time delay from C to *Bending* in Fig. 1.7. Moreover, when sinusoidal wave input is entered to generate hysteresis loop of the SMA actuators, the obtained hysteresis loops for same input value are inconsistent. Tested system input is

$$u = 3\sin(t\omega\pi - 0.5\pi) + 3 \tag{2.15}$$

where ω is 1/15 Hz. For the input, sine wave is shifted by 0.5π so the wave starts at its minimum value. Even when the output values are averaged, the shape of hysteresis loop is not consistent in terms of the shape and the slope of curves.

These properties pose great challenge for the accurate dynamics modeling.

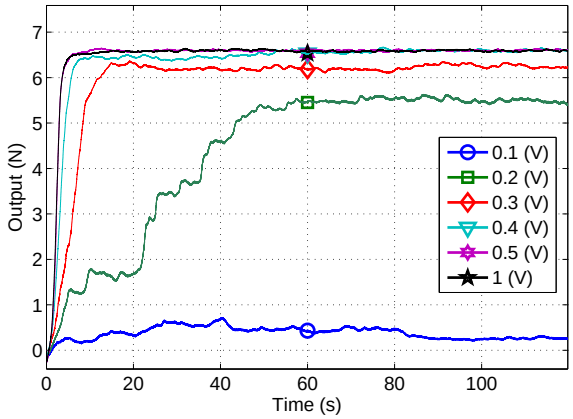

(a) Step response test results

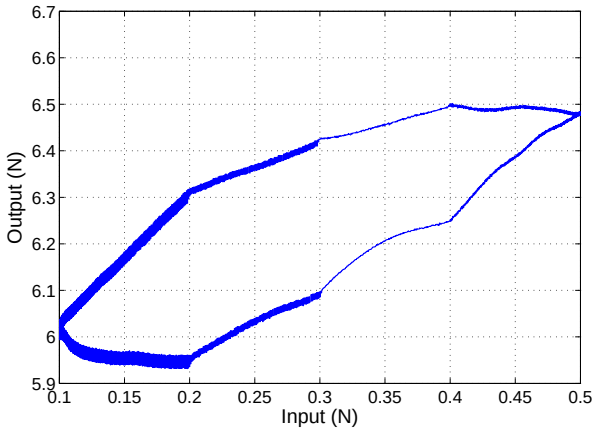

(b) Hysteresis loop obtained from sine wave response

Fig. 2.6 Responses of SMA actuators to PWM input

In order to observe the hysteretic behavior more precisely, system input is changed from digital to analog signal. It allows the user to enter voltage as input to generate specific current to drive the SMA actuators. Voltage to current

converter (Fig. 1.6) introduced in Section 1.3 is used. The conversion is expressed as

$$I = \frac{V}{R} \tag{2.16}$$

where I is current, V is voltage, and resistance R has value of 11 Ω. Resistance of 11 Ω is specifically selected because maximum supply voltage generated by Ectron board is ±10 V. The resistance R allows to generate current from 0 to 660 mA, the maximum current that can be applied to a SMA actuator, with limited voltage range of the system. The the maximum voltage is limited to be 7 V. Step and sinusoidal responses are re-evaluated with analog system input and displayed in Fig. 2.7. The response is more stable and less noisy compared to Fig. 2.6 (a). Also the hysteresis loop is more defined than the digital input system.

In addition, heating and cooling response test reveals fastest heating and cooling time. Maximum and minimum voltages are applied for this study. From Fig. 2.8, it can be approximated that the maximum heating takes 3 seconds and the complete cooling from the maximum tension takes 10 seconds. Heating is faster than the cooling because heating is actively controlled with the power supply and cooling depends on natural air convection only.

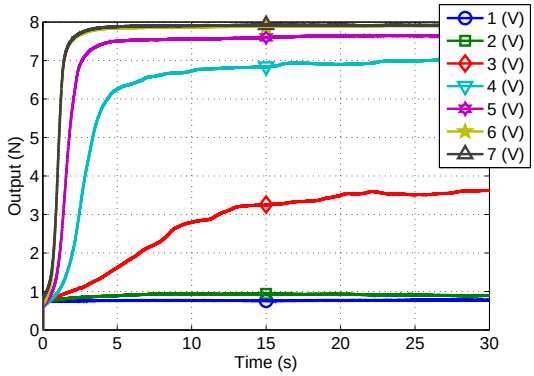

(a) Step response test results

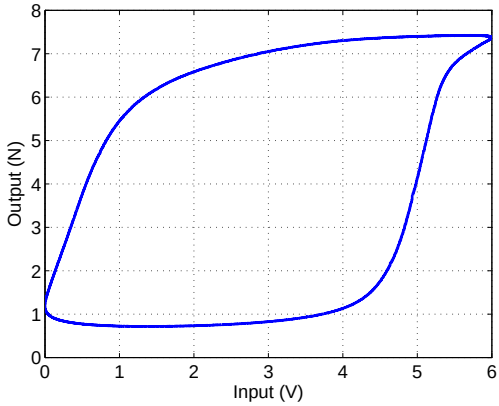

(b) Hysteresis loop obtained from sine wave response

Fig. 2.7 Responses of SMA actuators to analog input

2.2.2 Classical Preisach Model

Preisach model is one of the most commonly used model to simulate the hysteresis of SMA. It assumes that the system consists of a parallel summation of a continuum of weighted hysteresis operators. Each relay hysteron has input and

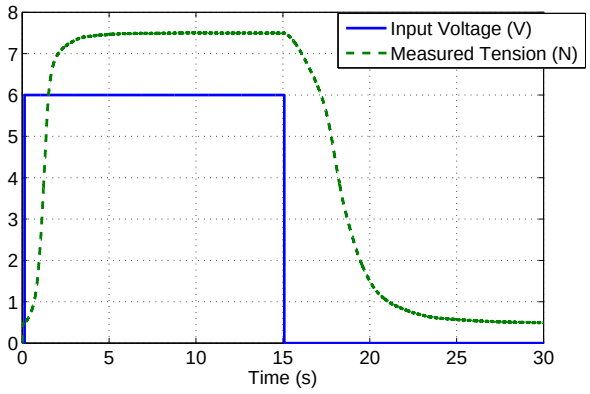

Fig. 2.8 Heating and cooling time of SMA actuator

output that form a loop corresponding to switch-on (up), and to switch-off (down). As input value changes, Preisach model switches plane and adjusts output value between 0 and 1. Then the output values are multiplied by the corresponding weight $\mu(\alpha, \beta)$. The Preisach model is expressed as

$$y(t) = \iint_{\alpha \geq \beta} \mu(\alpha, \beta) \gamma_{\alpha,\beta}[u(t)] d\alpha d\beta \tag{2.17}$$

where $\gamma_{\alpha,\beta}$ denotes Preisach plane switching operator.

Identification of the plane switching operator and the weight function has to be made to fit specific cases. In this section, Preisach model implementation method is explored along with the simulation results.

Discretization of the Preisach Plane

Preisach plane is triangular shape area on α and β graph where α ¿ β. α and β imply switch on and off threshold of a relay. On the Preisach plane, range of α and β is defined by the minimum and maximum input range as:

$$P(\alpha, \beta) = \{\text{range} : u_{minimum} \leq \beta \leq \alpha \leq u_{maximum}\} \tag{2.18}$$

In practice, Preisach plane has to be discretized in order to divide the plane into finite number of elements. In discretized Preisach operator, more accurate data can be obtained by using bigger array of data for α and β. However, it can cause slowness of system. Discretization level L determines the number of discretized Preisach plane cells and natural location of α and β. Preisach plane is divided uniformly into L rows and columns obtaining K cells where K is [9]

$$K = \frac{L(L+1)}{2} \tag{2.19}$$

Then α and β values at i-th location are [9];

$$\alpha_i = \beta_i = u_{min} + (i-1)\left(\frac{u_{max} - u_{min}}{L}\right) \tag{2.20}$$

As L increases, the accuracy of the model increases. However, this will slow the system down since high L value creates more elements to be analyzed.

For discretized Preisach model, the output is expressed as

$$y(n) = \sum_{i=1}^{L} \sum_{j=1}^{i} \gamma_{ij}(n)\mu_{ij} \tag{2.21}$$

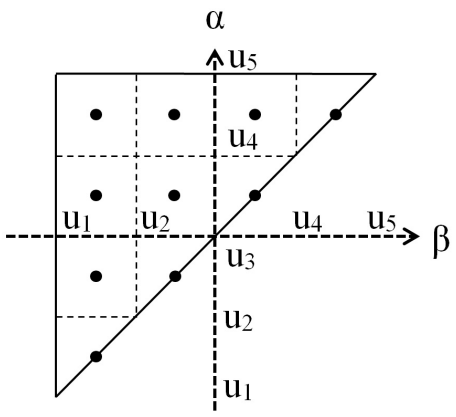

Fig. 2.9 Discretization of Preisach plane (L=4)

where i and j denotes the location of α and β, and γ denotes the Preisach operator (1 or 0).

Preisach Operator

Discretized Preisach plane cells alternative their values between 1 and 0 depending on their input value. As discussed in Section 2.1.2, Preisach operator can be expressed as

$$\gamma_{\alpha,\beta} = \begin{cases} 0, & \text{if } u \leq \beta \\ 1, & \text{if } u \geq \alpha \\ \text{r}, & \text{if } \beta < u < \alpha \end{cases} \tag{2.22}$$

where r is 1 if u_{t-1} is greater than α, and 0 if u_{t-1} is less than β. As input u increases, Preisach plane boundary parallel to β axis increases (see Fig. 2.10(a): P^+ area is increasing along with the boundary u_1, parallel to β axis) and as u decreases, plane boundary parallel to α axis decreases (see Fig. 2.10(b): P^+ area is

decreasing along with the boundary u_2, parallel to α axis). These plane boundaries are called memory curves.

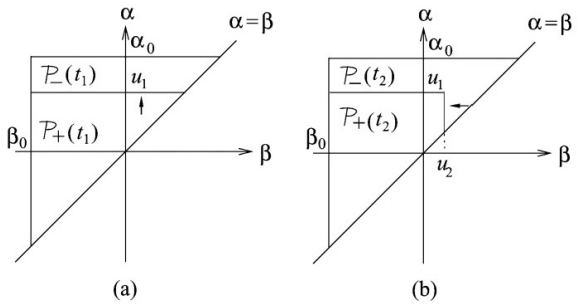

Fig. 2.10 Memory curve on Preisach plane [9]

Preisach Weight Function

As defined in Eq. (2.17), Preisach model is the integral of weight function and Preisach operator over Preisach plane. It suggests one to one relationship between weight function and Preisach operator and that weight function must be mapped on predetermined discretized Preisach plane. It is important to select a weight function and its parameters since it defines shape and size of the hysteresis. Derivative-Arc-Tangent (DAT) offers a simple and easy method to form the density function. Parameters in DAT are easy to find in hysteresis loop by simple measurements. Even though it is similar to Gaussian and Lorrentzian function, sharing four same parameters (refer to Section 2.1.2), having one more extra term, η, allows more flexibility. Additional η term defines the corners of the hysteresis loop. DAT weight

function is defined as

$$\mu_{DAT}(\alpha, \beta) = \frac{A}{1 + \{[(\alpha + \beta)\sigma_1]^2 + [(\alpha - \beta - h)\sigma_2]^2\}^{\eta}} \tag{2.23}$$

where A is a normalization factor, and h and σ are the characteristic parameters of distribution [29]. Fig. 2.11 shows the plotted weight function where color bar represents the μ value. Those parameters can be defined by observing the hysteresis loop.

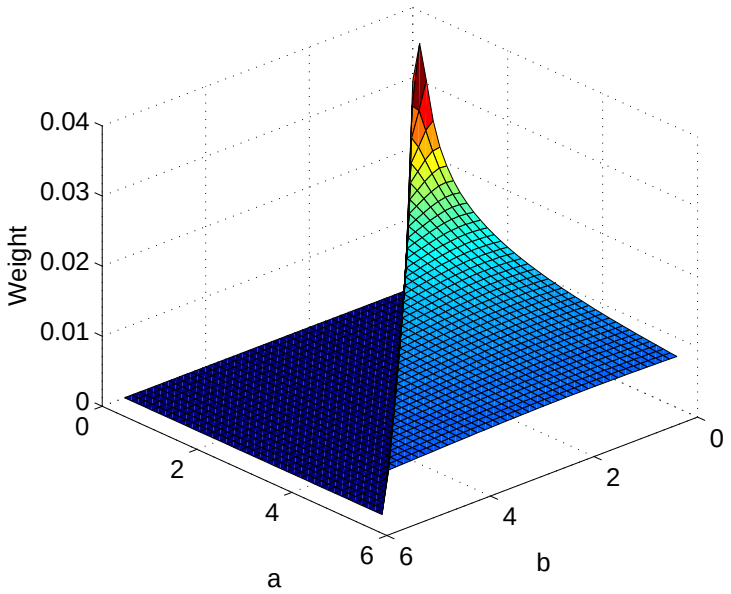

Fig. 2.11 Weighting function

2.2.3 Maxwell Resistive Capacitor

Maxwell resistive capacitor (MRC or Maxwell model) has been used to map the nonlinearity between displacement and force in piezoelectric actuators (PEA) [8,41]. Even though it is not widely used for hysteresis mapping of SMA actuator, Maxwell model is a good modeling tool since hysteresis loops of SMA actuator and PEA have the similar shape. One major difference is that the location of where hysteresis forms. SMA has hysteresis between temperature and force, while the hysteresis of PEA is between displacement and force. Therefore, input is treated as the displacement of Maxwell elements to allow the model to map the hysteresis of SMA actuator.

Maxwell Slip Element

Maxwell model is a parallel connection of Maxwell slip elements. A Maxwell slip element, also referred to elasto slide element, is imaginary component composed of a massless block attached to a spring. When a block is moved back and forth, hysteresis occurs. When a block is moved forward, force increases. However, once the breakaway force of a spring is reached, force cannot increase anymore but displacement can still increase. Same applies to a block moving in negative direction. Displacement-force behavior of a Maxwell slip element is illustrated in Fig. 2.5 (a).

Modified Maxwell Slip Element

Hysteresis of SMA actuators has asymmetric shape and irregular curves. In order to accurately accommodate these complexity, two major modifications are made. Breakaway force has two different boundaries, maximum and minimum, and unconventional springs with two stiffnesses are used. Both changes cannot be explained by physical spring-mass system. Conventional Maxwell model has breakaway force boundaries $\pm f_b$ depending on the direction of spring motion. It is expressed as

$$f_b = -k\Delta \tag{2.24}$$

where f_b is breakaway force, k is spring constant and Δ is the maximum deformation of spring. This allows symmetric upper and lower boundaries. By allowing to have different absolute values of the maximum breakaway force, f_{max}, and the minimum breakaway force, f_{min}, boundaries accommodate the asymmetric shape of hysteresis. Different boundary forces mean different elements are activated for the same magnitude change in positive and negative direction. It allows the model to have different elements acting for different directions therefore asymmetric hysteresis loop can be formed. For this research, Maxwell elements are divided into two groups. One group is activated only when the direction of the applied force is positive and the other group acts when the direction of the force is negative. Also,

each spring is assumed to have two spring stiffnesses: one for increasing curve, k_{inc}, and the other for decreasing curve, k_{dec}. If boundaries are symmetric, slope would be constant therefore it is important to have asymmetric boundaries for each element to model the hysteresis of irregular shape . Some elements have negative spring stiffness. This offers more flexible slope change to adapt to hysteresis loop better. Initial rising curve is disregarded since it is affected by internal state. It is unstable and not meaningful to model. After the modification, force equation becomes

$$F_i = \begin{cases} k_{i_{inc}}(x - x_{b_i}), & \text{if } 0 < (x - x_{b_i}) \\ k_{i_{dec}}(x - x_{b_i}), & \text{if } (x - x_{b_i}) < 0 \\ f_{i_{max}}, & \text{if } f_{i_{max}} \leq k_{i_{inc}}(x - x_{b_i}) \\ f_{i_{min}}, & \text{if } k_{i_{dec}}(x - x_{b_i}) \leq f_{i_{min}} \end{cases} \tag{2.25}$$

The mathematical description for coding purpose is,

$$\delta_i(t+1) = \begin{cases} k_{i_{inc}}[x(t+1) - x(t)] + \delta_i, & \text{positive stick} \\ k_{i_{dec}}[x(t+1) - x(t)] + \delta_i, & \text{negative stick} \\ \delta_{i_{max}}(t), & \text{positive slip} \\ \delta_{_{min}}(t), & \text{negative slip} \end{cases} \tag{2.26}$$

These modifications allow the model to have different slopes for increasing and decreasing curves. Therefore the model is flexible and easy to adjust for un-smooth curve. Fig. 2.12 shows the hysteresis of a single Maxwell element. After modifications, increasing and decreasing curves no longer have the same slope.

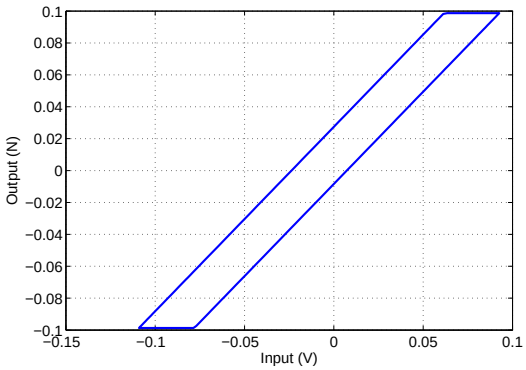

(a) Normal hysteresis

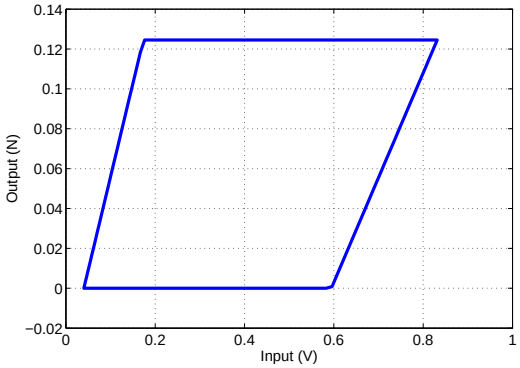

(b) Modified hysteresis

Fig. 2.12 Maxwell slip element

2.3 Parameter Identification

2.3.1 Data Collection

In order to verify the model parameters, experimental data is collected from the test facility introduced in Section. 1.3 to compare with the simulated data. The input is fed through the open loop system. Data collection is conducted with

repeating full sinusoidal wave and decaying sinusoidal wave to examine the entire spectrum of input range with increasing and decreasing values. Two sets of sinusoidal wave that were used as input signal are displayed in Figs. 2.13 (a) and 2.14 (a). The full sinusoidal input wave is

$$u = 3\sin(t\omega\pi - 0.5\pi) + 3 \tag{2.27}$$

Desired input voltage range is 0 to 6 V. Since wave has amplitude 3 which is shifted upward by 3. Also sine wave is phase shifted by 0.5π so that the wave starts from 0. Multiple sets of data are collected from the same input and averaged for analysis purpose in order to reduce the noise. Open loop test results are illustrated in Figs. 2.13 (b) and 2.14 (b).

The hysteresis loop obtained from the open loop experiments is frequency dependent. When decaying sinusoidal wave tests are run with five different frequencies, its frequency dependency is illustrated in Fig. 2.15 as shapes of the hysteresis loop are clearly different.

2.3.2 Initial Parameter Calculation

Normally, parameters in the hysteresis models represent physical characteristics of the hysteresis loop. For example, sharpness of the hysteresis loop and saturation point are some of them. In order to successfully estimate initial parameters, it is crucial to study properties of hysteresis loop. Initial parameter identification is

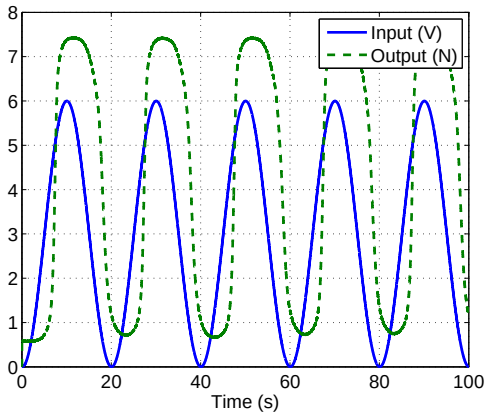

(a) Time vs. Input and Output

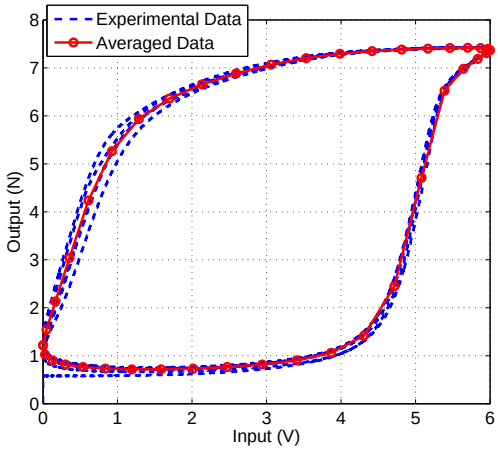

(b) Hysteresis Loop

Fig. 2.13 Experimental data of a SMA actuator

considered as a rough estimate before optimization. The initial parameters have to be re-adjusted because they are obtained from analyzing the major hysteresis loop only, which has limited range of data. For this research, the initial parameters are obtained by measuring the specific points and slopes of the hysteresis curve and its

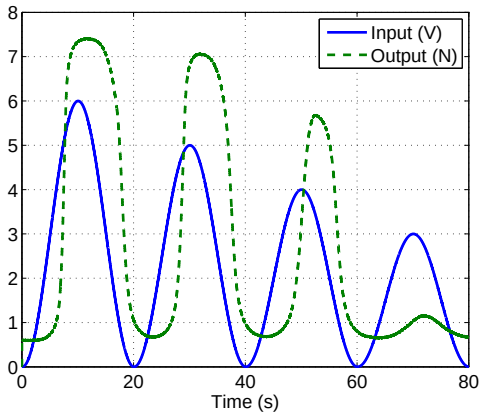

(a) Time vs. Decaying Input and Output

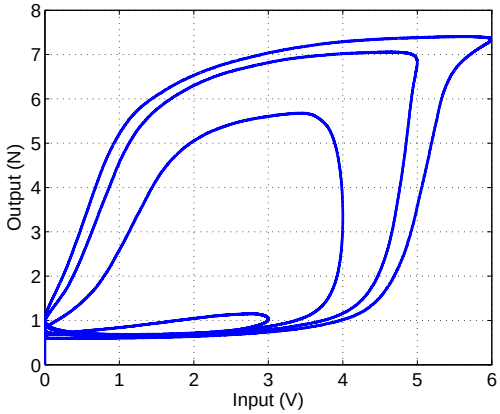

(b) Hysteresis loops

Fig. 2.14 Test results of decaying sinusoidal input

initial rising curve. Parameter identification methods for Classical Preisach model and Maxwell model are introduced in this section.

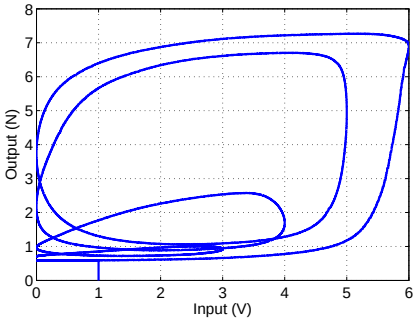

(a) Hysteresis loop at 1/10 Hz

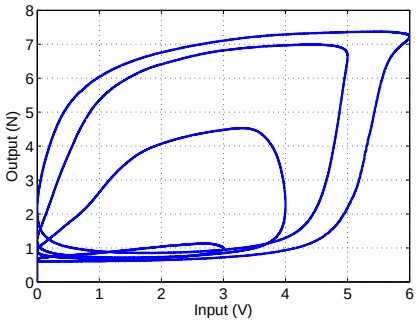

(b) Hysteresis loop at 1/15 Hz

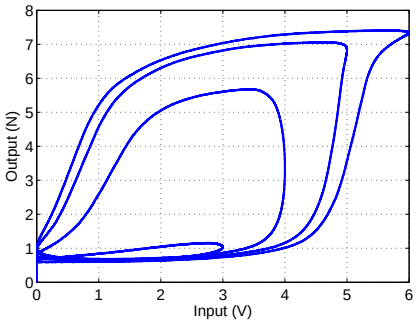

(c) Hysteresis loop at 1/20 Hz

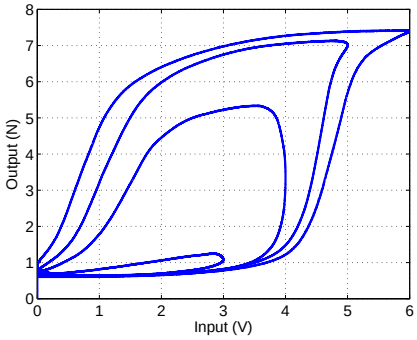

(d) Hysteresis loop at 1/25 Hz

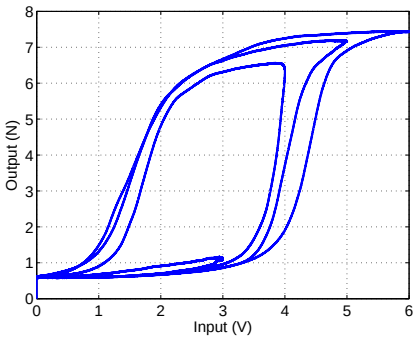

(e) Hysteresis loop at 1/50 Hz

Fig. 2.15 Frequency dependency (hysteresis at different frequencies)

Preisach Parameter Identification

Preisach model is proposed to identify the hysteresis in ferromagnetic material. Therefore, the names of parameters and terms have magnetism references. The weight function determines the shape of the hysteresis therefore some characteristic points on the measured curve are utilized. They are plotted in Fig. 2.16.

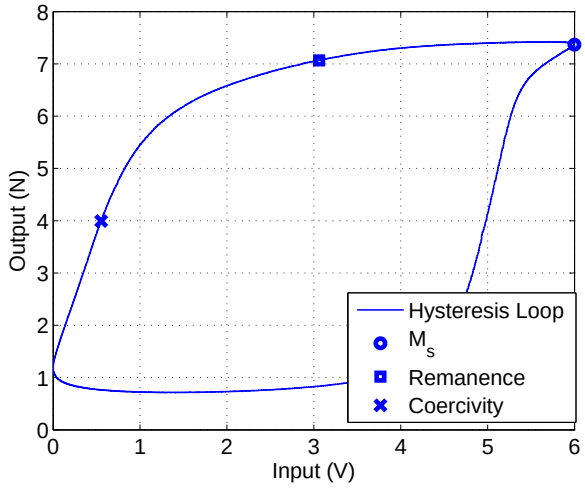

Fig. 2.16 Hysteresis loop characteristic points

M_s is called saturation magnetization which is the maximum magnetization value. Coercivity is when magnetization value drops to half point after saturation, and a point on the hysteresis curve where the applied input is half of its amplitude is called remanence.

The shape of hysteresis loop is determined by the weight function. Selected weight function, DAT, requires five parameters to be identified: h, σ_1, σ_2, A, and

η. All parameters are described in Section 2.1.2. Parameters of DAT can be easily determined by measuring the hysteresis loop.

$$\mu_{DAT}(\alpha, \beta) = \frac{A}{1 + \{[(\alpha + \beta)\sigma_1]^2 + [(\alpha - \beta - h)\sigma_2]^2\}^\eta} \tag{2.28}$$

The parameter h is the coercivity. The parameters σ_1 and σ_2 determine the slope of the hysteresis loop at the coercivity by:

$$\sigma = \sqrt{\sigma_1^2 + \sigma_2^2} \tag{2.29}$$

Also the ratio σ_1 and σ_2 determines the height of minor loops vis-a-vis the major loop. The parameter A can be simply calculated from

$$A = \frac{1}{4\pi\sigma_1\sigma_2} \tag{2.30}$$

Lastly, η is roughly estimated by plugging in a number and adjusting from comparing the results with the experimental data.

Maxwell Parameter Identification

Goldfarb and Calanovic [8] offer steps to obtain necessary parameters for MRC. Their method is closely followed and the same notations are used in this section. Two parameters, spring stiffness and breakaway force, need to be identified to complete Maxwell model. In order to calculate the stiffness, piecewise linear fit of the initial rising curve of the hysteresis is obtained. Number of segments from a

rising curve fit determines the number of Maxwell slip elements. If n segments are obtained, n Maxwell slip elements are required. Before conducting mathematical process, it should be noted that the SMA system does not have distinctive initial rising curve. Thus, an imaginary initial curve is made up to estimate the initial parameters.

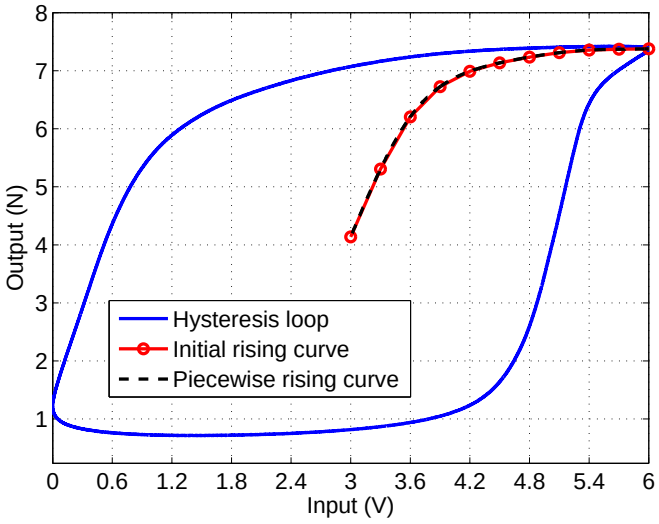

Fig. 2.17 Initial rising curve

Once the initial curve is approximated, it is fitted by evaluating piecewise polynomial. As demonstrated in Fig. 2.17, the modified curve follows the initial rising curve closely in piecewise form. The step of obtaining piecewise initial curve is important because the piecewise initial curve allows easy measurements of slopes on the initial curve. Each point on the piecewise curve is uniformly distributed along the input axis. Slope of a rising curve can be expressed with the following

spring stiffness

$$s_j = \sum_{i=j}^{n} k_i \tag{2.31}$$

where s represents the slope, k_i is the spring stiffness of the i-th Maxwell element. It can be rearranged in a matrix form as

$$s = Ak \tag{2.32}$$

where s is $n \times 1$ vector of the segment slopes, A is a $n \times n$ upper triangular matrix of ones, and k is a $n \times 1$ vector of Maxwell model spring stiffness. Finally, to obtain the spring stiffness, it is rewritten as

$$k = A^{-1}s \tag{2.33}$$

On a displacement vs. force graph, the location of segments is

$$x_j = \frac{f_j}{k_j} \tag{2.34}$$

where f_j is the breakaway force of the j-th Maxwell element. With all the information obtained from the previous steps, the breakaway force can be evaluated as

$$f = Kx \tag{2.35}$$

where f is a $n \times 1$ vector of the breakaway forces, K is a $n \times n$ diagonal matrix of the spring stiffnesses, and x is a $n \times 1$ vector of the segment locations. The last breakaway force, located at $f(n, 1)$, has to be considerably larger than the rest of the breakaway forces to avoid the saturation.

2.3.3 Parameter Optimization

Initial parameters of both Preisach and Maxwell models need to be optimized for accurate modeling. New sets of data with varying amplitude input are utilized for optimization. Parameters are optimized by using least square method of output discrepancy.

$$\min \sqrt{\sum (y_{ex} - y_m)^2} \tag{2.36}$$

where y_{ex} is the output obtained from experiments and y_m is the model output. Optimization of the parameters are performed by MATLAB function: 'fmincon'. Its optimization process is as follows:

(a) Specify the desired input and output

(b) Provide initial parameters to be optimized, lower and upper boundaries, and error tolerance

(c) The program runs iterations

(d) As the program runs, it compares values experiment data and simulation data and calculates least square error

(e) The program adjusts parameter within lower and upper boundaries to reduce error

(f) The program runs until error cannot be reduced by set tolerance and provides optimized parameters

The process is also explained in a flow chart in Fig. 2.18, where u represent input, v is output, $para$ is parameter to be optimized, lb and ub are the lower and upper bound, $MaxIter$ is the maximum number of iteration, $TolFun$ is a parameter for the error tolerance and v_m is the model output.

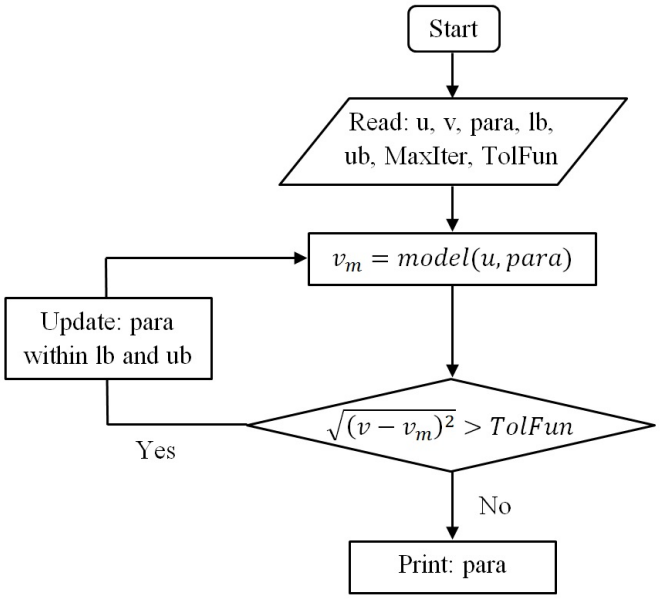

Fig. 2.18 Optimization flowchart

2.4 Model Verification

Two hysteresis models are verified in two steps: a) preliminary and b) simulation tests. The preliminary test is a simple single amplitude test that focuses on the

model's ability to adapt to the general shape of hysteresis loops. The simulation test is the second step to take after the preliminary test. It is performed to determine how well the model adjusts to the different amplitudes. Both, the Preisach and the Maxwell, model outputs are compared with the experimental data and each other.

2.4.1 Preliminary Results

Preliminary results from both Preisach and Maxwell models are obtained from the single amplitude single frequency sinusoidal wave of the potential difference input. Same data set used for the initial parameter identification is utilized.

Classcial Preisach Model

The discretized weight function displayed in Fig. 2.11 has asymmetric surface and Preisach operator has memory effect. It suggests that while Preisach model can follow the asymmetric shape of the hysteresis loop, it cannot track the irregular changing slope of a hysteresis curve. The result is as expected since the weight function is the deciding factor of hysteresis shape and size. Preliminary test results are displayed in Fig. 2.19.

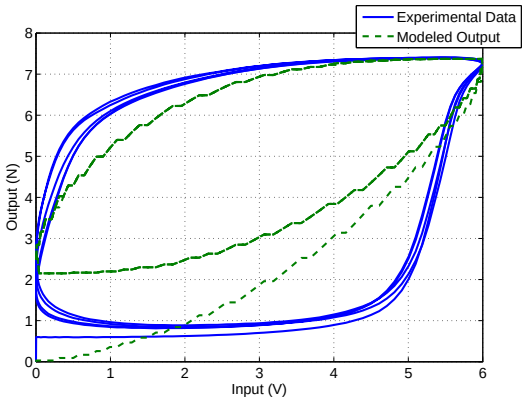

(a) Hysteresis loop comparison

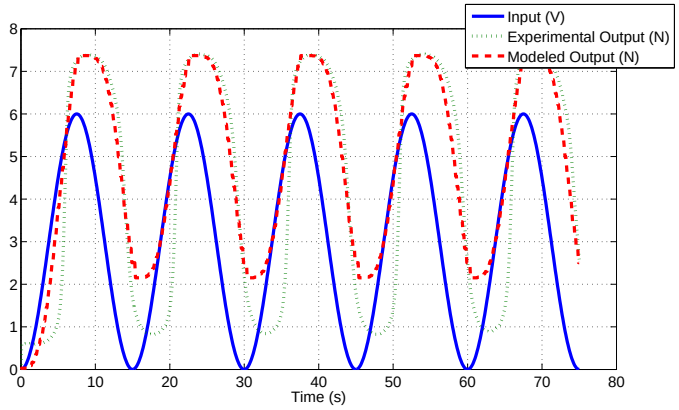

(b) Time (s) vs. Output (N)

Fig. 2.19 Hysteresis analysis by classical Preisach model

Maxwell Model

Maxwell model has multiple elements working individually. Each element provides different output for the same input, making it easier to adjust to different slopes with increasing and decreasing curves for hysteresis loop. Fig. 2.20 shows model output has changing slope on both increasing and decreasing curves due

to the modifications. Since the saturated hysteresis loop is symmetric shape with smooth curve, Maxwell slip elements have the same increasing and decreasing spring stiffness.

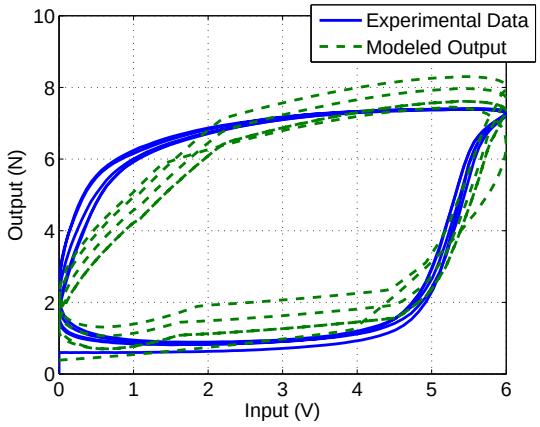

(a) Hysteresis loop comparison

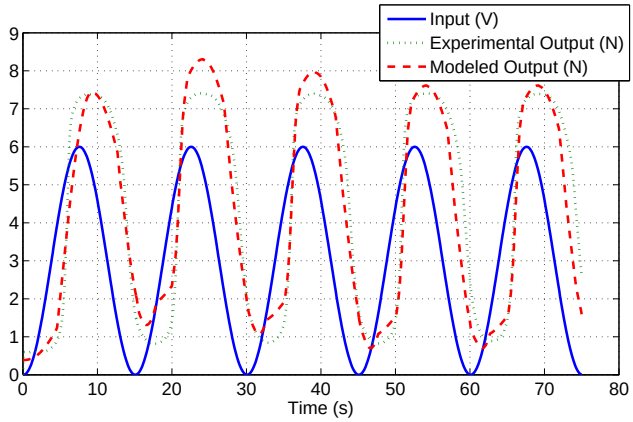

(b) Time (s) vs. Output (N)

Fig. 2.20 Hysteresis analysis by Maxwell model

2.4.2 Simulation Results

Preliminary results reveal that the Maxwell model produced better fit of hysteresis loop than that of the classical Preisach model. The Maxwell model is more flexible and has faster process time than the Preisach model as well. In order to confirm that the model can accommodate various amplitudes and frequencies, simulations with decaying sinusoidal wave with different frequencies are performed. Tested frequencies are $\omega = 1/10$, $1/15$, $1/20$, $1/25$, $1/50$ Hz.

Parameters are optimized for $\omega = 1/15$ Hz therefore as frequency changed, accuracy was affected. It should be noted that the parameter can be optimized for different frequencies depending on the application. While both models follow the general trend of data, Maxwell model does not only model the different amplitudes and frequencies better but also performs faster than the Preisach model.

2.5 Conclusions

While both Preisach and Maxwell models are suitable for modeling hysteresis loop, Maxwell model clearly shows its strength in modeling asymmetric unconventional hysteresis curve. Maxwell also has faster execution time. It is expected because of the amount of data processing involved in the Preisach model such as evaluation of Preisach plane switching, and calculation with weighting function each

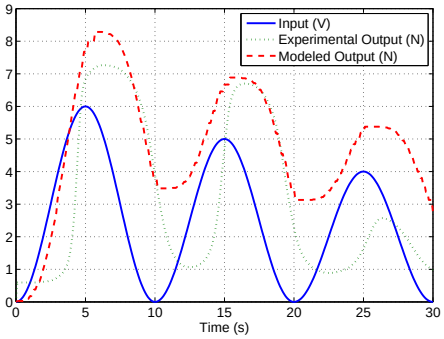

(a) Modeled output (N) at $\omega = 1/10$ Hz

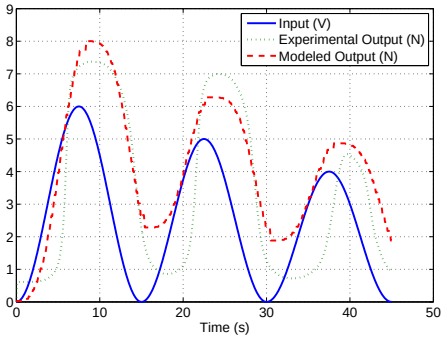

(b) Modeled output (N) at $\omega = 1/15$ Hz

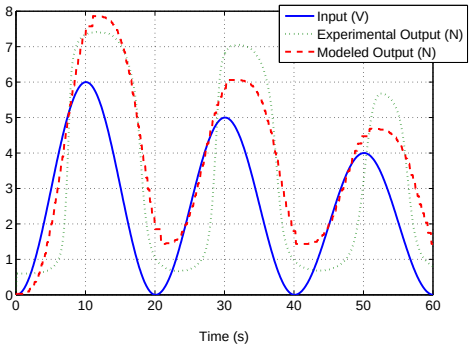

(c) Modeled output (N) at $\omega = 1/20$ Hz

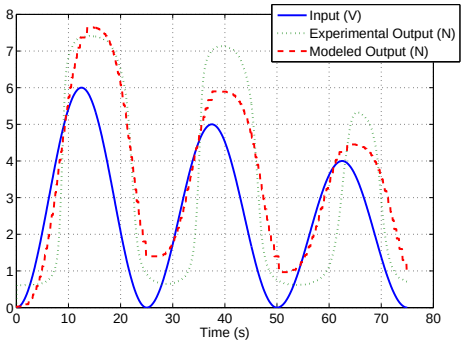

(d) Modeled output (N) at $\omega = 1/25$ Hz

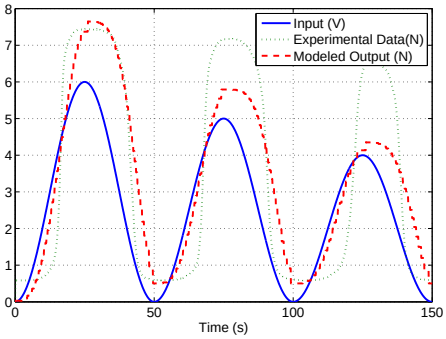

(e) Modeled output (N) at $\omega = 1/50$ Hz

Fig. 2.21 Simulation results of the Preisach model

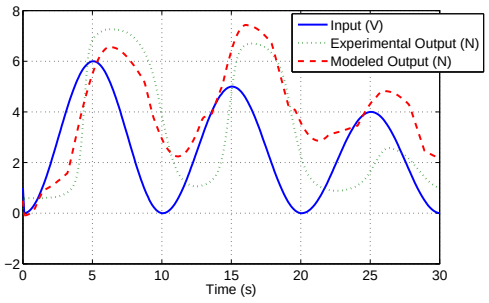

(a) Modeled output (N) at $\omega = 1/10$ Hz

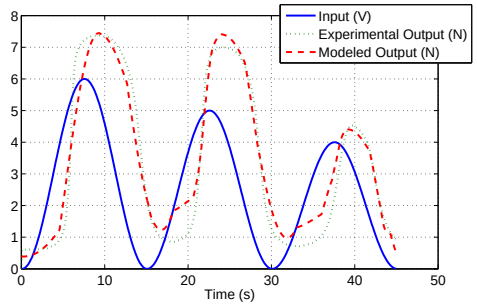

(b) Modeled output (N) at $\omega = 1/15$ Hz

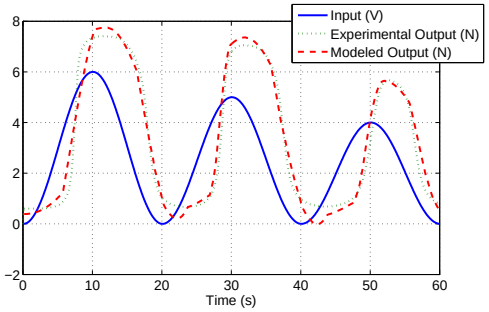

(c) Modeled output (N) at $\omega = 1/20$ Hz

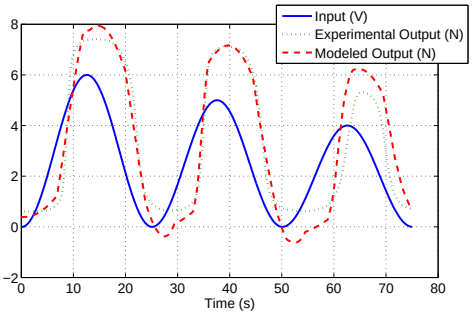

(d) Modeled output (N) at $\omega = 1/25$ Hz

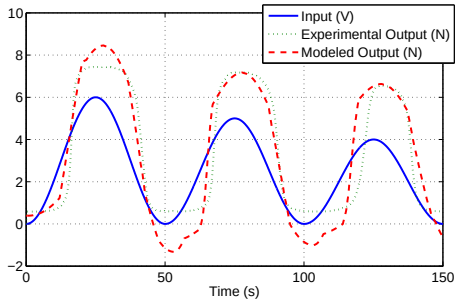

(e) Modeled output (N) at $\omega = 1/50$ Hz

Fig. 2.22 Simulation results of the Maxwell model

time when input changes. Even with higher discretization level of Preisach model, Maxwell model has better performance.

3 Control System Design

3.1 Background

Various linear and nonlinear controllers are introduced in this section. There has been great effort contributed by researchers to the control of the nonlinear SMA actuator system. Different types of control systems are designed to adapt to or compensate for the nonlinearity.

3.1.1 Linear Controllers

Linear controllers are usually coupled with an extra component to compensate for hysteresis since linear controller itself cannot compensate for the nonlinearity in SMA. Common controllers include simple PID feedback controller paired with the dynamics model of the system in the feedforward loop, PW modulated PID controller, and PID-P^3 controller. Hysteresis modeling predicts the desired input and output values, PWM has an advantage of energy saving while maintaining positioning accuracy, and PID-P^3 is similar to PID controller with one extra term

which makes its implementation simple.

Hysteresis compensation model based controllers

Hysteresis model based linear controller has been researched by many researchers [26,28,42,43]. Hysteresis models compensate for hysteresis behavior in smart materials and reduce the tracking error. Majima et al. [42] suggest a control system which is a combination of PID feedback loop and a feedforward loop. Feedforward loop obtains the desired input and output values from the modified classical Preisach model. Another advantage of having a feedforward loop with hysteresis model is once the model is established, there is no need for complicated control system. A simple feedback controller such as PID controller can be used to correct the modeling error since the nonlinearity has already been taken care of by the model. Ge and Jouaneh [28] also performed a simulation with the generalized Preisach model in the feedforward loop coupled with a PID controller for piezoceramic actuators.

PID-P^3

Shameli et al. [44] proposed a novel PID-P^3 controller to compensate for the hysteresis and perform a piecewise position control. The suggested PID-P^3 controller is [44],

$$u(t) = K_p e(t) + K_I \int_0^t e(\tau) d\tau + K_D \dot{e}(t) + K_T [e(t)]^3 \tag{3.1}$$

It has one more term than a typical PID controller, $K_T[e(t)]^3$, which contains a cubic term of the position tracking error. This term has considerable effects on reducing the settling time and overshoot of the system. For large error, the controller provides great control effort and for small error, the cubic term almost vanishes and the controller works as a standard PID controller.

Control with PWM

PWM control is a choice for energy sensitive application. Ma et al. [45] suggest to use PWM as system input to reduce the energy consumption by the SMA actuators. Simulation results were compared with those using PD controller to demonstrate its energy efficiency. PWM is selected over other modulators because it is robust to disturbances and easy to implement using microprocessors. Accurate PWM control design is crucial in order to identify the input time and displacement relationship.

3.1.2 Nonlinear Controller

Due to the nonlinearity that exists in SMA, nonlinear controller would be the natural choice. Unlike linear controllers with hysteresis compensation, nonlinear controller offers a direct solution. Its ability to eliminate or reduce the nonlinear effects of the hysteresis allows to improve the performance of the system.

Sliding Mode Control

SMC is usually used when there are uncertainties in nonlinear dynamic systems [10]. Elahinia et al. [46] adopted a sliding mode controller (SMC) to calculate the desired stress of the SMA wire with a single degree of freedom. Simulations reveals that its performance is more suitable than a PID controller for vibration control and dealing with uncertainties and noises. Lee and Ahn [47] utilized a hyperbolic tangential sliding mode control (SMC) and time delay estimation (TDE). The hyperbolic tangential sliding surface specifies the nonlinear error dynamics and yields an accurate and chattering-free control while the TDE provides simplicity and robustness to the controller in spite of the hysteresis effect of the SMA.

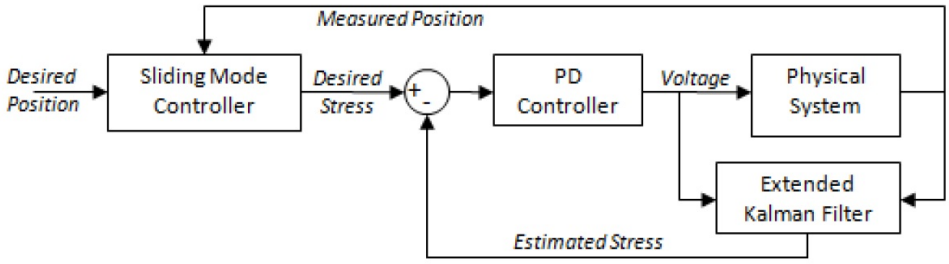

Fig. 3.1 Sliding mode control system [10]

Fuzzy Logic Control

Fuzzy logic controller (FLC) is one of the many algorithms used for nonlinear systems. It employs a relatively simple mechanism that constructs nonlinear

controllers via the use of heuristic information [11]. Many researchers have used this method for the hysteretic behavior of the control of shape memory alloy. Ahn and Nguyen [11] suggested a self-tuning Fuzzy PID controller. It adjusts P, I, and D gains using Fuzzy interface. Fuzzy interface examines its feedback value and determines the PID gains based on evaluation.

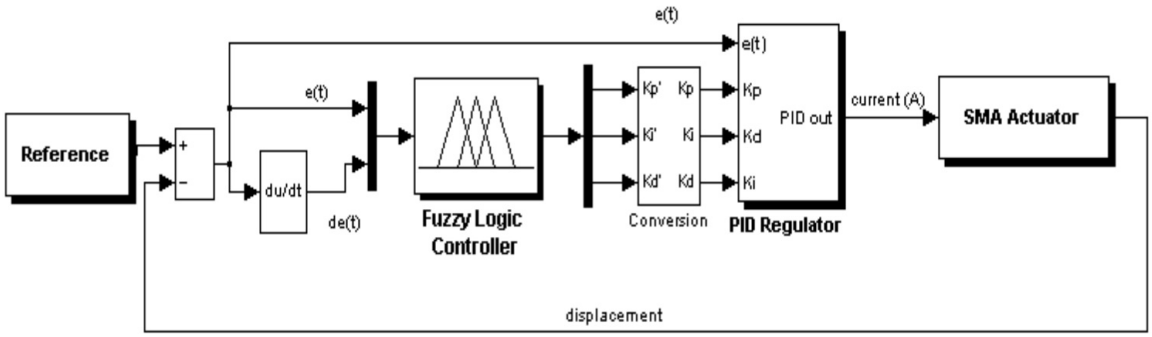

Fig. 3.2 Self tuning fuzzy PID controller [11]

Segmented Discrete State Control

Selden et al. [12] implemented a new approach of dividing the smart material into segments and control them separately. Segmented discrete state control analyzes the SMA wire which is divided into segments and applies individual control effort to each segment as a group of finite state machines. Each segment has two states, hot or cold, and the total displacement is proportional to the number/length of 'hot' elements. It is almost like digital signal control with two main concepts of

segmentation and binary control. The controller provides robust and stable result, however, heating and cooling time of each segments is long and energy consumption is large.

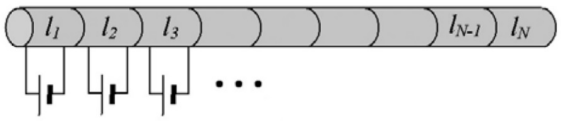

Fig. 3.3 Segmented SMA elements [12]

3.2 Controller Design

In nonlinear system, feedback controller is simply not enough. There are several methods to improve the performance of the controller. Addition of feedforward controller is a simple and effective way to significantly improve the controller. Feedforward controller provides the knowledge of the system through dynamics modeling independent of the system feedback. It allows the system to receive stable input regardless. It prevents the system from having fluctuation and relieves the control effort of feedback controller since it only has to correct the modeling error and disturbance.

An accurate feedforward controller generally requires accurate dynamics modeling that may cost good amount of time and resources. However, it has benefits that outweigh the disadvantages. It is easy to implement and provides consistent

control quality with high speed. It usually has lower energy consumption than other controllers that leads to low operating costs. In addition, when the dynamics model is accurate, it only requires simple feedback controller for correcting error to significantly improve the performance without jeopardizing the stability. It is typically used with feedback controller to correct unmeasured/unmodeled disturbances.

The control system used in this research is illustrated in Fig. 3.4 (a). It is a combination of two controllers and it has been used with proven performance. Dynamics model of the SMA actuator (Fig. 3.4 (b)) is inversed and implemented in an open loop feed-forward controller for hysteresis compensation. The role of the inverse model is to predict input value $u(t)$ for user entered desired output tension; $y_d(t)$ is provided. The inverse model reduces the hysteresis effect and linearizes the system. It is discussed in more detail in Section 3.3. Since Maxwell model closely maps the hysteresis of SMA actuators, a simple feedback controller, such as PI controller, can be utilized to correct the modeling error and improve control accuracy. Also, PI-P^3 controller is designed and used to demonstrate the improvement with feedforward controller and the effect of P^3 term.

$$\begin{aligned} \text{PI-P}^3: &\quad u(t) = K_p e(t) + K_I \textstyle\int_0^t e(\tau)d\tau + K_T[e(t)]^3 \\ \text{PI}: &\quad u(t) = K_p e(t) + K_I \textstyle\int_0^t e(\tau)d\tau \end{aligned}$$

Controller gains are obtained by trial and error with several configuration sets. Some restrictions are made to controllers. From the step response test in Fig. 2.7, input value of 1 V does not have impact on the system and if the current exceeds

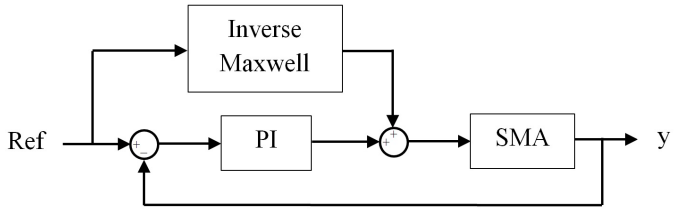

(a) Feedforward combined with PI controller in closed loop

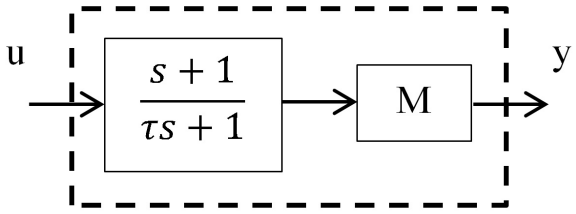

(b) Dynamic compensator and Maxwell model

Fig. 3.4 Control system design

660 mA (Table. 1.1), the SMA wires burn out. Range of the applicable voltage is determined to be 1 - 7 V, therefore, the system output is limited to stay within the range. Also feedforward controller is turned off when measured tension is greater than the desired tension. This is because the feedforward controller puts control effort regardless of the system state. Sometimes it introduces excessive system input. In order to prevent unnecessary overshoot, feedforward controller is activated to contribute only when the system needs more effort.

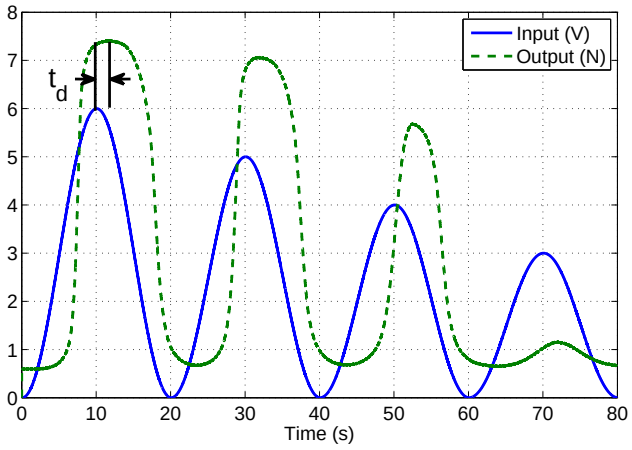

Fig. 3.5 Sinusoidal response of SMA (t_d is time delay)

3.2.1 Dynamic Compensator

SMA actuators have slow response speed and cause a positive phase shift, where the output leads the input. It takes approximately 3 seconds to fully reach the maximum tension (Fig. 2.8) and sinusoidal wave test reveals 2 seconds time delay between the input and output signal. This delay is constant through out the sinusoidal response tests. In order to compensate for this, a first order lead compensator is designed using the time constant, τ of the SMA system

$$C(s) = \frac{s+1}{\tau s+1} \tag{3.2}$$

τ is estimated to be 5 and optimized to be 4.28 for this research.

3.2.2 Hysteresis Compensation Based on Inverse Maxwell Model

Hysteresis models can be used in a feedforward control loop and compensate for the nonlinear hysteresis effect in a SMA actuator. Depending on the system setup, an user can select the original and/or inverse model to determine the dynamics. Between two selected hysteresis modeling methods, previous section has proved that the Maxwell model is more effective. Therefore only the inverse Maxwell model is developed.

Formulation of the Inverse Maxwell Model

Inverse model can be developed by tracing the Maxwell model algorithm back. As mentioned in Section 2.1.2, force distribution is proportional to spring stiffness value, only when the element(s) is not saturated. It is assumed that the initial displacement x_0 and the initial force F_0 is 0. When the inverse model takes in its first set of data, current force and previous force, $CurF$ and $LasF$ in Fig. 3.6, it analyses the change in magnitude and direction of force. This step is performed to choose which spring stiffness can be utilized. There are two sets of spring stiffness for increasing and decreasing input force, denoted as $IncSS$ and $DecSS$. The model determines the saturated elements by comparing the maximum U_{max} and the minimum U_{max} boundary forces. After the unsaturated elements are identified,

the program distributes increased/decreased force, ΔF to remaining unsaturated elements. Then, the program checks if there are additional saturated elements. If no more element is saturated, it produces displacement as output (all unsaturated elements have the same displacement). If not, it runs another iteration to redistribute the force.

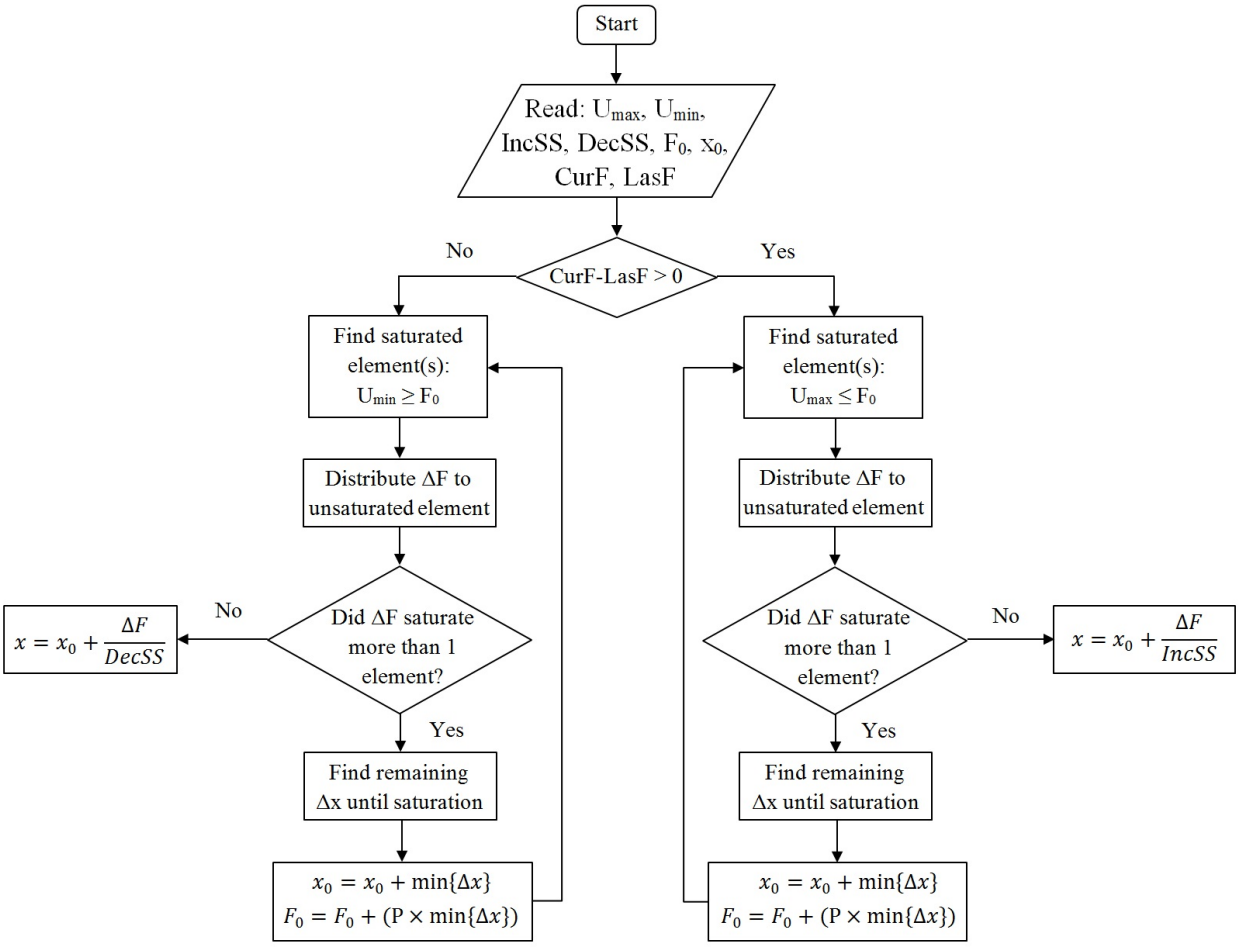

Fig. 3.6 Flowchart of inverse model algorithm

There is one condition that has to be satisfied in order to have successful inverse

model. The sum of the parameters must not change its direction (positive to negative or negative to positive) during the iteration. The fundamental function in Maxwell model indicates that the force of individual element is

$$F_i = \frac{k_i}{\sum k} x_i \tag{3.3}$$

where F is the force, k is the spring constant, x is the displacement, and i represent the i-th element. It has to be noted, while iteration, direction of x elements do not change. If the $\sum k$ direction changes, it forces x elements to change direction and ultimately causes singularity. When it occurs, the inverse model fails to process and all the calculation becomes incorrect after the singularity point.

The flowchart in Fig. 3.6 starts off by reading the maximum and minimum boundaries, the spring stiffnesses, and the initial force and displacement of each Maxwell element. Then it calculates if $CurF$ is greater or less than $LasF$ to determine the direction of the system. When the current force is greater, the increased force is distributed among the Maxwell elements. If one or more Maxwell elements are positively saturated, it redistributes the remaining forces among the unsaturated elements and this cycle continues until the increased force is fully distributed. Same process is applied for the negative ΔF with negative saturation level.

Verification

Naturally, it is desired to have the inverse model that can trace model output back to its system input. Fig. 3.7 shows that the inverse model output matches with the input of the Maxwell model when Maxwell model output is used as the inverse model input. Then the inverse model is combined with the Maxwell model to linearize the hysteresis.

3.3 Experimental Results

Experimental verifications are performed to compare several different controllers including feedback-feedforward controller to feedback controller itself and PI to PI-P^3 in order to demonstrate the effects of inverse Maxwell model on the control system and extra P^3 term. Five different frequency tests are performed along with the step response test for feedforward, feedback, and feedback and feedforward combined controller. Frequencies of 1/10, 1/15, 1/20, 1/25, and 1/50 Hz are used for five peak-to-peak sinusoidal waves.

$$u(t) = 3\sin(t\omega\pi - \pi/2) + 3 \tag{3.4}$$

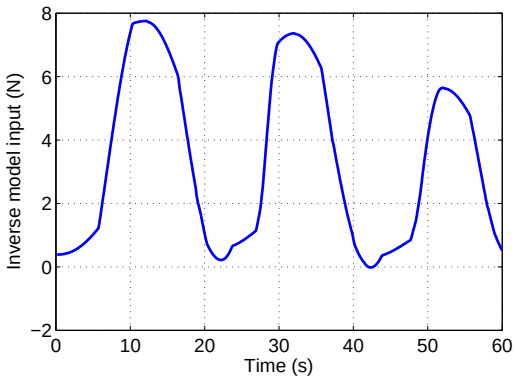

(a) Input (V) of inverse Maxwell

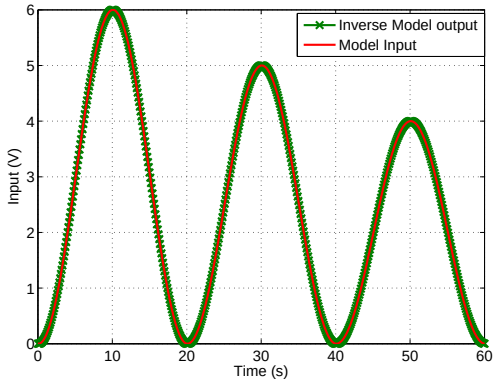

(b) Comparison of output of inverse Maxwell model with input of Maxwell model

Fig. 3.7 Inverse Maxwell model verification

3.3.1 Feedforward Controller

First, the experiments of feedforward controller are conducted. It is apparent, even by eyes, that the hysteresis effect is reduced when the results, displayed in Fig. 3.9, are compared with open loop experiment data in Fig. 2.15. As the model

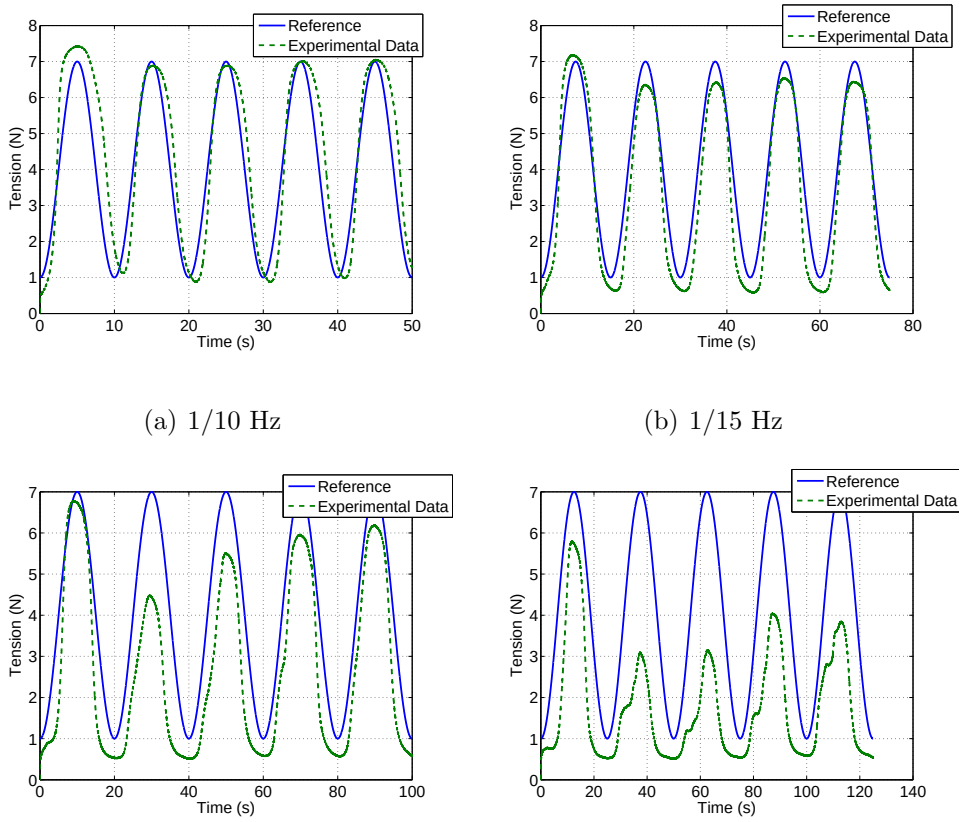

(a) 1/10 Hz

(b) 1/15 Hz

(c) 1/20 Hz

(d) 1/25 Hz

Fig. 3.8 Hysteresis with different sinusoidal wave input and feedforward controller

is optimized for 1/15 Hz, the best performance is achieved at 1/15 Hz. The performance quality drops significantly as frequency decreases. Fig. 3.9 shows the hysteresis is reduced the most at $\omega = 1/15$ Hz. If the application calls for slow frequency, parameters of the model can be readjusted. The hysteresis is frequency dependent so it is hard to have one solid model to cover the entire frequency range. As it can be observed in Fig. 3.8, it can only cover small frequency range. However,

the model still follows the general trend.

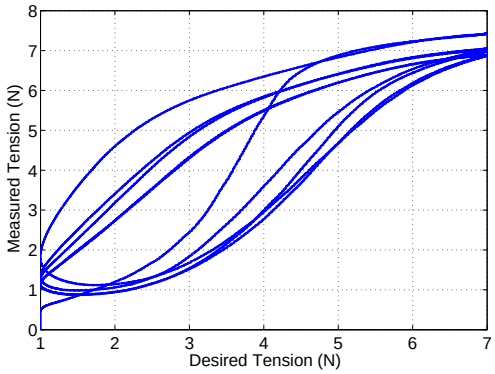

(a) 1/10 Hz hysteresis loops

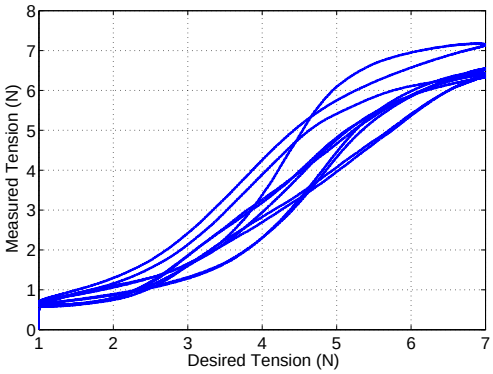

(b) 1/15 Hz hysteresis loops

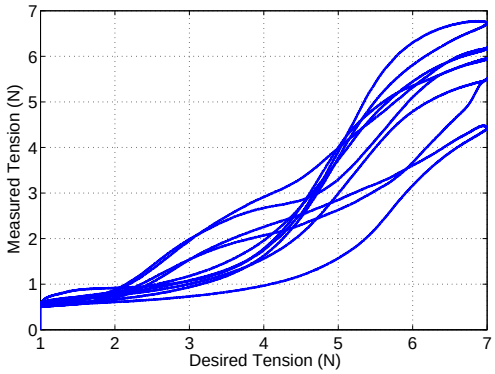

(c) 1/20 Hz hysteresis loops

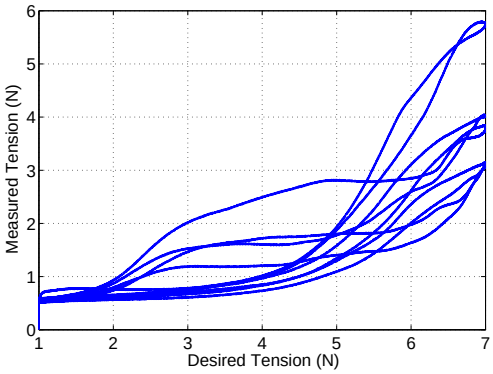

(d) 1/25 Hz hysteresis loops

Fig. 3.9 Hysteresis with different sinusoidal wave input and feedforward controller

3.3.2 Feedback Controller vs. Feedforward-Feedback Controller

This section presents sinusoidal wave test and step response test results. The difference is more visible when the frequency is high. As frequency decreases, the

performance of the feedback controller has visibly increased (refer to Fig. 3.9). It is observed that the hysteresis loop gets thinner as frequency decreases (refer to Fig. 2.15). It allows the feedback controller to improve its accuracy without any improvements or modifications. The test results are displayed in Figs. 3.10-3.13. The improvement is most visible at $\omega = 1/10$ Hz (Fig. 3.10). The response time is faster and the combined controller follows the desired value more closely than the feedback controller alone. Even at $\omega = 1/50$ Hz in Fig. 3.12 where it is hard to observe the difference, settling time is still visibly faster.

The impact on reducing the hysteresis effect of the feedforward controller is also evident in step response test, as shown in Fig. 3.13. The overshoot for both heating and cooling is reduced, settling time is improved, and the system oscillates less when it reached the desired value.

3.4 Conclusions

Hysteresis modeling and its effectiveness in control system have been presented in this paper. The Maxwell model is selected to map the hysteresis loop of the SMA actuator. Maxwell model is a simple and effective method to identify the hysteresis in SMA actuators and has faster computation speed than the classical Preisach model. Hysteresis curves in SMA actuators in the experimental setup are asymmetric and nonlinear. Modifications made in elasto-slide elements offer

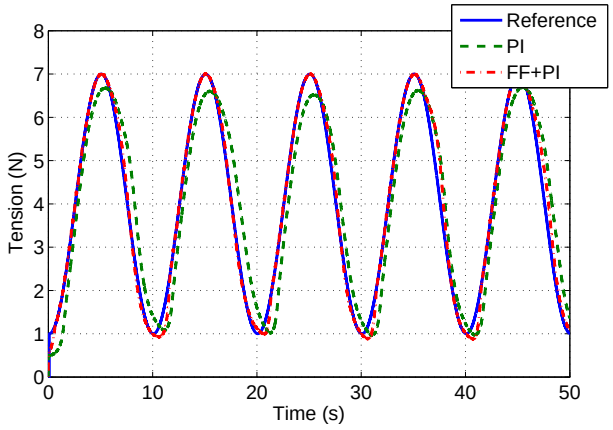

(a) Comparison between PI and feedforward+PI controllers

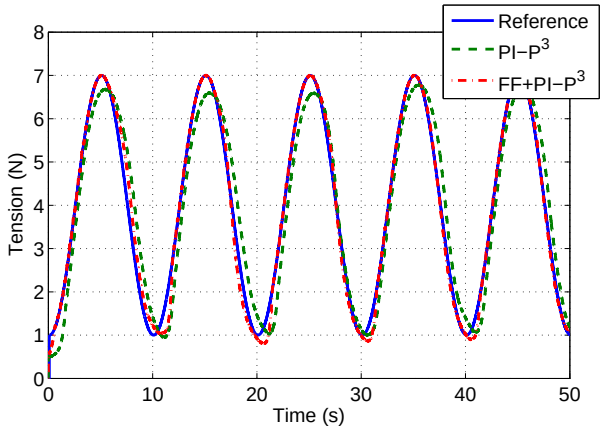

(b) Comparison between PI-P^3 and feedforward+PI-P^3 controllers

Fig. 3.10 Test results of 1/10 Hz sinusoidal wave

flexibility in modeling to provide accommodations for irregularity.

Inverse Maxwell model is developed and implemented in feedforward controller to compensate for nonlinearity and linearize the system. A controller that combines feedforward controller and feedback controller is proposed. Feedforward term

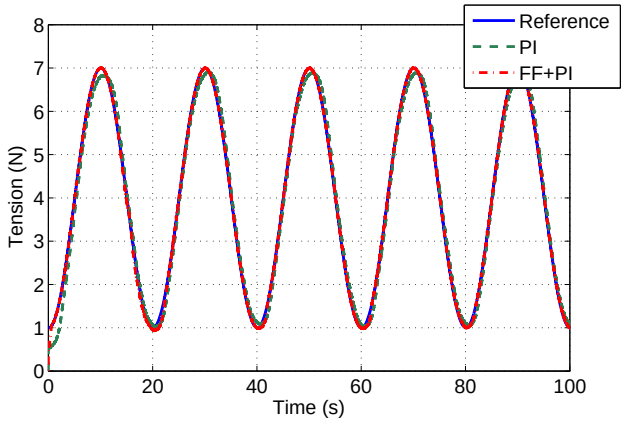

(a) Comparison between PI and feedforward+PI controllers

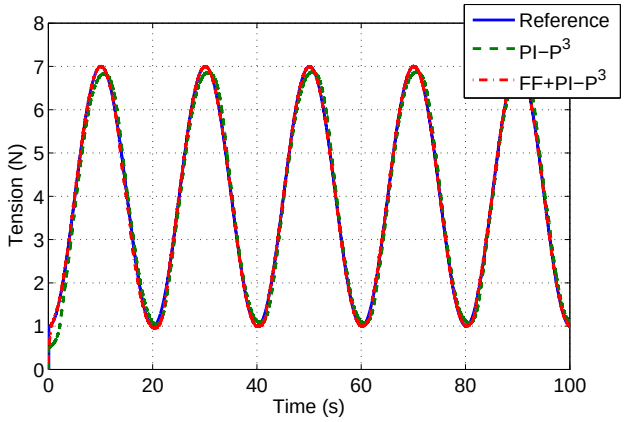

(b) Comparison between PI-P^3 and feedforward+PI-P^3 controllers

Fig. 3.11 Test results of 1/20 Hz sinusoidal wave

compensates for the hysteresis and feedback controller corrects the modeling error caused by the inverse Maxwell model. Experimental results show the improvement in tracking and hysteresis is suppressed effectively. Experimental output and model

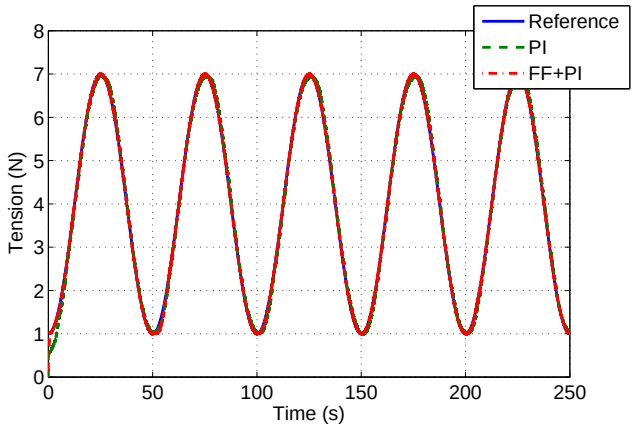

(a) Comparison between PI and feedforward+PI controllers

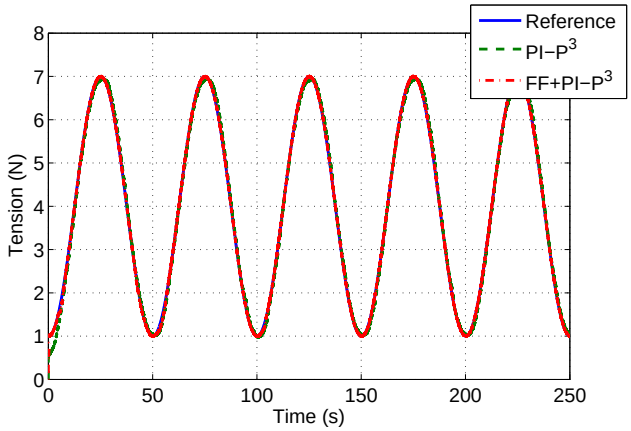

(b) Comparison between PI-P^3 and feedforward+PI-P^3 controllers

Fig. 3.12 Test results of 1/50 Hz sinusoidal wave

output are compared and sums of root mean square errors are obtained.

$$\mathrm{E}_{RMS} = \sqrt{\frac{\sum_{i=1}^{n}(y_{exp_i} - y_{model_i})^2}{n}} \tag{3.5}$$

where E_{RMS} is root mean square error, y_{exp} is experimental output, and y_{model} is model output. Analysis of sums of root mean square errors listed in Table. 3.1

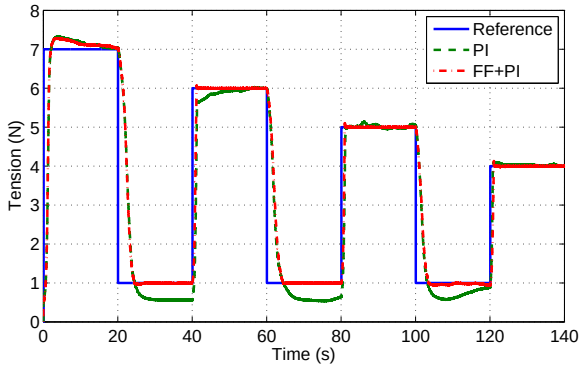

(a) Comparison between PI and feedforward+PI controllers

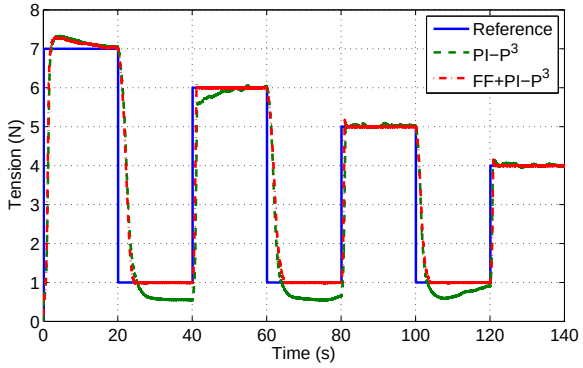

(b) Comparison between PI-P^3 and feedforward+PI-P^3 controllers

Fig. 3.13 Test results of step response

suggest that the performance has improved by 67-74% when feedforward term is added for all frequencies. SMA actuators have slow response time. The performance improves as the frequency decreases. Even though it is hard to see visible difference between PI and PI-P^3, the RMS error clearly shows that the PI-P^3 performs better for all the tested frequencies and step response test. Test errors are displayed in

Figs. 3.14-3.16

Table 3.1 Root mean square error (E_{RMS}) with different controllers

Controller type	Frequency (Hz)					Step
	1/10	1/15	1/20	1/25	1/50	
FF	4.67×10^{-3}	2.60×10^{-3}	2.89×10^{-3}	3.14×10^{-3}	3.10×10^{-3}	3.63×10^{-3}
PI	4.49×10^{-3}	1.53×10^{-3}	7.95×10^{-4}	5.08×10^{-4}	1.77×10^{-4}	3.17×10^{-3}
Feedforward + PI	2.99×10^{-3}	3.24×10^{-4}	2.02×10^{-4}	1.35×10^{-4}	6.08×10^{-5}	3.02×10^{-3}
PI-P^3	4.38×10^{-3}	1.46×10^{-3}	7.14×10^{-4}	4.63×10^{-4}	1.51×10^{-4}	3.14×10^{-3}
Feedforward + PI-P^3	1.41×10^{-3}	1.69×10^{-4}	1.84×10^{-4}	7.67×10^{-5}	3.86×10^{-5}	2.96×10^{-3}

It is interesting to observe that, even though the accuracy of the feedforward controller decreases as the frequency increases, the result reveals that the best control effort is achieved when the frequency is 1/50 Hz. It is due to the nature of the SMA actuator that it has slow response time. Even though feedforward controller does not put much controller effort, feedback controller has enough time to adjust itself since the desired change is more gradual than other frequencies.

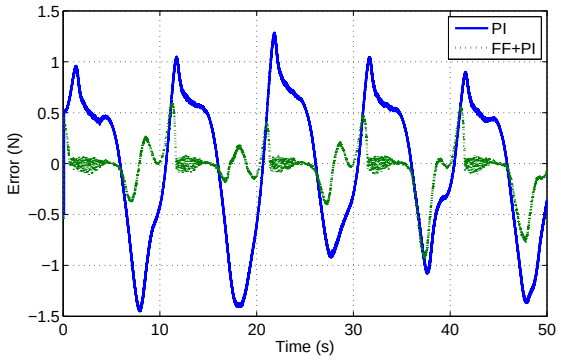

(a) Error at 1/10 Hz

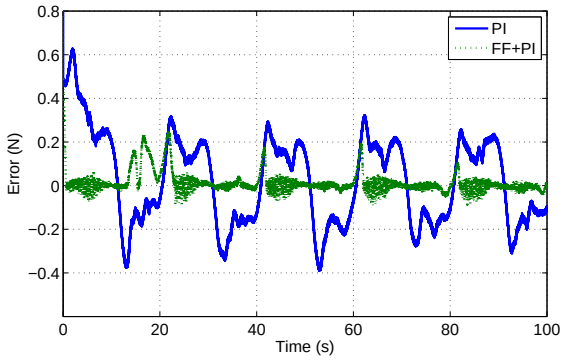

(b) Error at 1/20 Hz

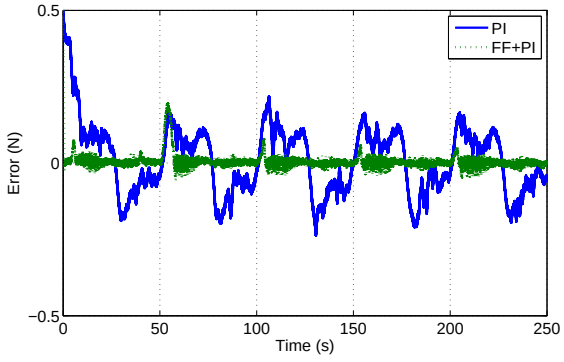

(c) Error at 1/50 Hz

Fig. 3.14 Error comparison of PI and feedforward+PI controllers

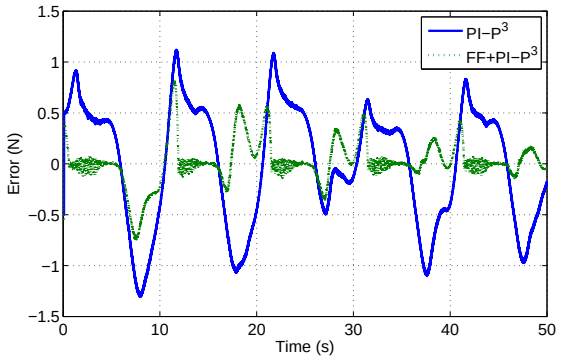

(a) Error at 1/10 Hz

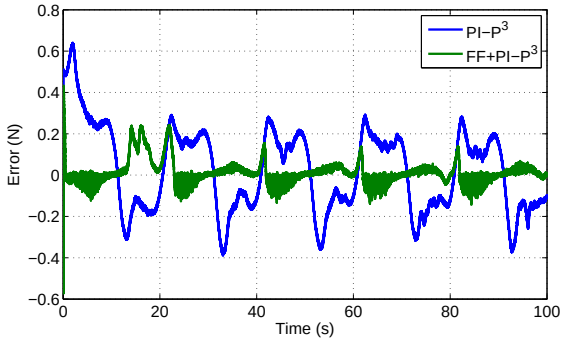

(b) Error at 1/20 Hz

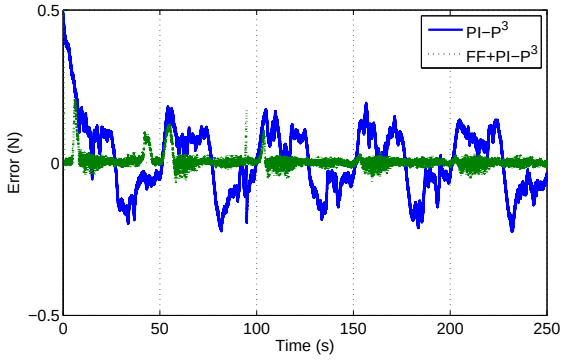

(c) Error at 1/50 Hz

Fig. 3.15 Error comparison of PI-P^3 and feedforward+PI-P^3 controllers

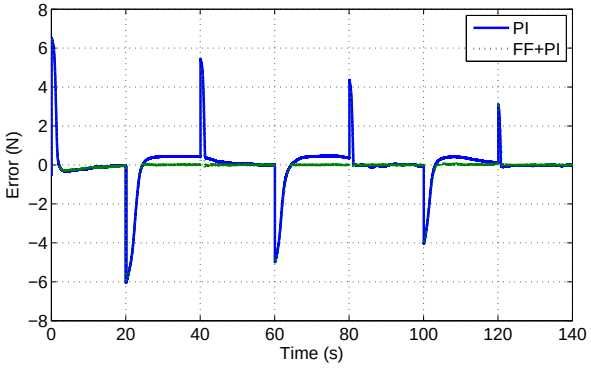

(a) PI and feedforward+PI controllers

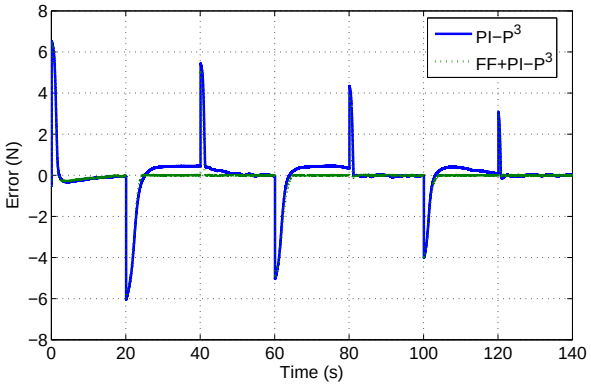

(b) PI-P^3 and feedforward+PI-P^3 controllers

Fig. 3.16 Error comparison of step response tests

4 Conclusions and Future Work

The main objective of this research is to develop an effective control system for SMA actuators that can be used in membrane system. Accurate tension control of SMA actuators allows the membrane system to maintain its flatness. It is accomplished by feedforward control with inverse dynamics model to compensate for hysteresis effect with a simple feedback controller.

The dynamics modeling offers a simple and effective solution for hysteresis compensation. Traditional and modified models, mainly classical Preisach model and modified Maxwell model, are studied based on dynamic effects of SMA actuators. Unconventional mass-spring system is suggested for flexible shape and curve fitting ability. Modified Maxwell model produced more accurate hysteresis curve, when it was compared with the experimental data, and had shorter computation time than that of the classical Preisach model. Since feedforward controller compensates for hysteresis, simple feedback controller can be used to correct the modeling error. Inverse modified Maxwell model is developed and implemented in feedforward

controller to compensate for the hysteresis and linearize the system. Feedforward term compensates for the hysteresis and feedback controller corrects modeling error caused by the inverse Maxwell model. Experimental results show that the improvements in tracking are achieved and hysteresis has been effectively suppressed when a feedforward term is added to the feedback controller. Also, adding an extra term to PI controller, namely PI-P^3 controller, has improved the accuracy further.

Future work involves further expanding the knowledge and technique of the SMA position control system design and implementing the developed system to membrane system.

Feedforward-feedback controller can be researched more in depth with various hysteresis modeling methods. Few options that can be studied further are to implement rate-dependent hysteresis models, and to establish the mathematical relationship between system input and output based on physical properties of SMA actuator, an alternative approach introduced in Section 2.1.2. Rate-dependent hysteresis model would be able to provide wider frequency coverage than rate-independent model. In addition, in this research, only one controller is explored. For the future research, it would be beneficial to explore broader control method such as adaptive and nonlinear controller.

The suggested controller works well with only one set of SMA actuators. There are few concerns and complications involved in broadening the scope of the research.

Challenges associated with the control implementation to membrane structure are

- Need to build more voltage to current converters for each set of SMA actuators or a group of SMA sets depending on the flatness control system design.
- Individual set of SMA actuators needs to be modeled for precision control. They all should be similar in theory however it is uncertain what effects non-modeled sets might cause.
- The membrane system is expected to operate in space. Model parameters need to be re-identified and adjusted in vacuum (and tested in the same environment).
- Cooling of the system relies on natural air convection. Active cooling system might be needed.

Bibliography

[1] Song, G., Chaudhry, V., and Batur, C., "Precision tracking control of shape memory alloy actuators using neural networks and a sliding-mode based robust controller," *Smart Materials and Structures*, Vol. 12, No. 2, 2003, pp. 223–231.

[2] Toru, S., "Fast and accurate position control of shape memory alloy actuators," Tech. rep., Australian National University (ANU), 2008.

[3] Sreekumar, M., Singaperumal, M., Nagarajan, T., Zoppi, M., and Molfino, R., "Recent advances in nonlinear control technologies for shape memory alloy actuators," *Journal of Zhejiang University Science A*, Vol. 8, No. 5, 2007, pp. 818–829.

[4] Orszulik, R. and Shan, J., "Membrane structure active flatness control using genetic algorithm with online objective reweighting," *Acta Astronautica*, Vol. 68, No. 11-12, 2011, pp. 2012–2024.

[5] Ahn, K. and Nguyen, B., "Internal model control for shape memory alloy actuators using fuzzy based Preisach model," *Sensors and Actuators A: Physical*, Vol. 136, No. 2, 2007, pp. 730–741.

[6] Hegewald, T., *Modellierung des nichtlinearen Verhaltens piezokeramischer Aktoren*, Ph.D. thesis, University Erlangen-Nuremberg, 2008.

[7] Muxworthy, A. and Roberts, A., *Encyclopedia of Geomagnetism and Paleomagnetism*, Springer, 2007.

[8] Goldfarb, M. and Celanovic, N., "Modeling piezoelectric stack actuators for control of micromanipulation," *IEEE Control Systems*, Vol. 17, No. 3, 1997, pp. 69–79.

[9] Tan, X. and Baras, J., "Adaptive identification and control of hysteresis in smart material," *IEEE Transactions on automatic control*, Vol. 50, No. 6, 2005, pp. 827–839.

[10] Chen, H., editor, *Shape Memory Alloys: Manufacture, Properties and Applications*, Nova Science Publishers, Inc, Hauppauge, NY, 2010.

[11] Ahn, K. and Nguyen, B., "Position control of shape memory alloy actuators using self tuning PID controller," *International journal of control, automation, and systems*, Vol. 4, No. 6, 2006, pp. 756–762.

[12] Selden, B., Cho, K., and Asada, H., "Segmented shape memory alloy actuators using hysteresis loop control," *Smart Materials and Structures*, Vol. 15, No. 2, 2006, pp. 642–652.

[13] Isaac, A., "Hysteresis," *The Elgar Companion to Radical Political Economy*, 1994.

[14] Peng, F., Jiang, X., Hu, Y., and Ng, A., "Actuation precision control of SMA actuators used for shape control of inflatable SAR antenna," *Acta Astronautica*, Vol. 63, No. 5-6, 2008, pp. 578–585.

[15] Peng, F., Jiang, X., Hu, Y., and Ng, A., "Application of SMA in membrane structure shape control," *IEEE Transactions on Aerospace and Electronic Systems*, Vol. 45, No. 1, 2009, pp. 85–93.

[16] Shu, S., Lagouda, D., Hughes, D., and Wen, J., "Modeling of a flexible beam actuated by shape memory alloy wires," *Smart Materials and Structures*, Vol. 6, No. 3, 1997, pp. 265–277.

[17] Lee, H. J. and Lee, J. J., "Evaluation of the characteristics of a shape memory alloy spring actuator," *Smart Materials and Structures*, Vol. 9, No. 6, 2000, pp. 817–823.

[18] Ishii, H. and Ting, K., "SMA actuated compliant bistable mechanisms," *Mechatronics*, Vol. 14, No. 4, 2004, pp. 421–437.

[19] Qin, C., Ma, P., and Tao, Q., "A prototype micro-wheeled-robot using SMA actuator," *Sensors and Actuators A: Physical*, Vol. 113, No. 1, 2004, pp. 94–99.

[20] Raparelli, T., Zobel, P. B., and Durante, F., "Design of a parallel robot actuated by shape memory alloy wires," *Materials Transactions*, Vol. 43, No. 5, 2002, pp. 1015–1022.

[21] Wang, X., Zheng, W., and Hu, Y., "Active flatness control of membrane structures using adaptive genetic algorithm," *Industrial and Commercial Applications of Smart Structures Technologies*, Vol. 6527, 2007.

[22] Tai, N. and Ahn, K., "Adaptive proportional-integral-derivative tuning sliding mode control for a shape memory alloy actuator," *Smart Materials and Structures*, Vol. 20, No. 5, 2011, pp. 54–59.

[23] Russell, R. and Gorbet, R., "Improving the response of SMA actuators," *Robotics and Automation*, Vol. 3, No. 9, 1995, pp. 2299 – 2304.

[24] Lewis, N., York, A., and Seelecke, S., "Experimental characterization of self-sensing SMA actuators under controlled convective cooling," *Smart Materials and Structures*, Vol. 22, No. 9, 2013, pp. 094012.

[25] Mayergoyz, I. D., *Mathematical model of hysteresis*, Springer, New York, 1991.

[26] Dutta, S. and Ghorbel, F., "Differential hysteresis modeling of a shape memory alloy wire actuator," *IEEE/ASME Transactions on Mechatronics*, Vol. 10, No. 2, 2005, pp. 189–197.

[27] Krasnoselskii, M. and Pokrovskii, A., *Systems with hysteresis*, Springer-Verlag, New York, 1989.

[28] Ge, P. and Jouaneh, M., "Generalized preisach model for hysteresis nonlinearity of piezoceramic actuators," *Precision engineering*, Vol. 20, No. 2, 1997, pp. 99–111.

[29] Consolo, G., Finocchi, G., Carpentieri, M., Cardelli, E., and Azzerboni, B., "About identification of scalar Preisach functions of soft magnetic materials," *IEEE Transactions on Magnetics*, Vol. 42, No. 4, 2006, pp. 923–926.

[30] Sutor, A. and Lerch, R., "A Preisach based model for the characterisation of magnetic hysteresis," *SENSOR TEST Conference*, Vol. 2, May 2009, pp. 65–70.

[31] Dobrota, C. and Stancu, A., "What does a first-order reversal curve diagram really mean? A study case: Array of ferromagnetic nanowires," *Journal of applied physics*, Vol. 113, No. 4, 2013, pp. 043928.

[32] Mayergoyz, I. D., *Mathematical Models of Hysteresis and Their Applications*, Elsevier, Boston, 2003.

[33] Rakotondrabe, M., "Classical Prandtl-Ishlinskii modeling and inverse multiplicative structure to compensate hysteresis in piezoactuators," *American Control Conference*, June 2012, pp. 1646–1651.

[34] Janaideh, M., Su, C., and Rakheja, S., "Development of the rate-dependent PrandtlIshlinskii model for smart actuators," *Smart Materials and Structures*, Vol. 17, No. 3, 2008, pp. 1–11.

[35] Brokate, M. and Sprekels, J., *Hysteresis and Phase Transitions*, Springer, Birlin, 1996.

[36] Fu, J., *On the adaptive controls of nonlinear systems with different hysteresis model presentations*, Ph.D. thesis, Concordia University, 2009.

[37] Royston, T. J. and Houston, B. H., "Modeling and measurement of nonlinear dynamic behavior in piezoelectric ceramics with application to 1-3 composites," *Journal of the Acoustical Society of America*, Vol. 104, No. 5, 1998, pp. 2814–2827.

[38] Bobbio, S., Mianio, G., Serpico, C., and Visone, C., "Models of magnetic hysteresis based on play and stop hysterons," *IEEE Transactions on Magnetics*, Vol. 33, No. 6, 2002, pp. 4417–4426.

[39] Rizos, D. and Fassois, S., "Presliding friction identification based upon the Maxwell slip model structure," *Chaos*, Vol. 14, No. 2, 2004, pp. 431–445.

[40] Nguyen, B. and Ahn, K., "Feedforward control of shape memory alloy actuators using fuzzy-based inverse Preisach model," *IEEE Transaction on control system technology*, Vol. 17, No. 2, 2009, pp. 434–441.

[41] Liu, Y., Shan, J., Gabbert, U., and Qi, N., "Hysteresis and creep modeling and compensation for a piezoelectric actuator using a fractional-order Maxwell resistive capacitor approach," *Smart Materials and Structures*, Vol. 22, No. 11, 2013, pp. 115020.

[42] Majima, S., Kodama, K., and Hasegawa, T., "Modeling of shape memory alloy actuator and tracking control stystem with the model," *IEEE Transactions on Control Systems Technology*, Vol. 9, No. 1, 2001, pp. 54–59.

[43] Tchoupo, G. and Leang, K., "Hysteresis compensation for high-precision positioning of shape memory alloy actuator using integrated iterative-feedforward and feedback inputs," *American Control Conference*, July 2007, pp. 4246–4253.

[44] Shameli, E., Alasty, A., and Salaarieh, H., "Stability analysis and nonlinear control of a miniature shape memory alloy for precise application," *Mechatronics*, Vol. 14, No. 5, 2005, pp. 471–486.

[45] Ma, N. and Song, G., "Control of shape memory alloy actuator using pulse width modulation," *Smart Materials and Structures*, Vol. 12, No. 5, 2003, pp. 712–719.

[46] Elahinia, M., Henneke, E., and Ahmadian, M., "Stress-based sliding mode control of a rotary SMA-actuated manipulator," *Smart Structures and Materials*, Vol. 5383, 2004, pp. 478–489.

[47] Lee, J., Jin, M., and Ahn, K., "Precise tracking control of shape memory alloy actuator systems using hyperbolic tangential sliding mode control with time delay estimation," *Mechatronics*, Vol. 23, No. 3, 2013, pp. 310–317.